Transportation Consortium of South-Central States

Tran-SET

Solving Emerging Transportation Resiliency, Sustainability, and Economic Challenges through the Use of Innovative Materials and Construction Methods: From Research to Implementation

Use of Nanoclays as Alternatives of Polymers Toward Improving Performance of Asphalt Binders

Project No. 17BASU01

Lead University: Arkansas State University

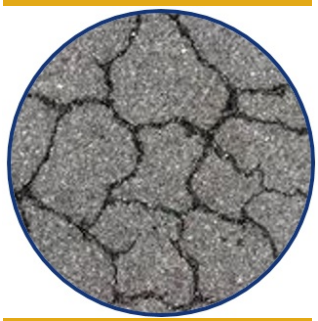

Enhancing Durability and Service Life of Infrastructure

Final Report

October 2018

Disclaimer

The contents of this report reflect the views of the authors, who are responsible for the facts and the accuracy of the information presented herein. This document is disseminated in the interest of information exchange. The report is funded, partially or entirely, by a grant from the U.S. Department of Transportation's University Transportation Centers Program. However, the U.S. Government assumes no liability for the contents or use thereof.

Acknowledgments

The authors acknowledge the Tran-SET for providing the financial support of this study. The authors also would like to thank Ergon, Inc., Memphis, TN for providing test materials for this study.

TECHNICAL DOCUMENTATION PAGE

1. Project No.	2. Government Accession No.	3. Recipient's Catalog No.
17BASU01		

4. Title and Subtitle	5. Report Date
Use of Nanoclays as Alternatives of Polymers Toward Improving Performance of Asphalt Binders	Oct. 2018
	6. Performing Organization Code
7. Author(s)	**8. Performing Organization Report No.**
PI: Dr. Zahid Hossain https://orcid.org/0000-0003-3395-564X Co-PI: Dr. Ashraf Elsayed https://orcid.org/0000-0003-1506-2784 GRA: Mohammad Nazmul Hassan https://orcid.org/0000-0003-3583-3101 GRA: MM Tariq Morshed https://orcid.org/0000-0002-2299-7011	
9. Performing Organization Name and Address	**10. Work Unit No. (TRAIS)**
Transportation Consortium of South-Central States (Tran-SET) University Transportation Center for Region 6 3319 Patrick F. Taylor Hall, Louisiana State University, Baton Rouge, LA 70803	**11. Contract or Grant No.** 69A3551747106
12. Sponsoring Agency Name and Address United States of America Department of Transportation Research and Innovative Technology Administration	**13. Type of Report and Period Covered** Final Research Report May 2017 – May 2018
	14. Sponsoring Agency Code

15. Supplementary Notes

Report uploaded and accessible at: Tran-SET's website (http://transet.lsu.edu/)

16. Abstract

The main goal of this study is to assess the feasibility of the use of nanoclay as an alternative to commonly used polymers such as styrene-butadiene-styrene (SBS), which are used to modify the performance grade (PG) of asphalt binders. Three types of nanoclay and two types of neat binders were selected for laboratory investigation. Different amounts (1, 2, and 3%) of nanoclays were used. A blending protocol has been developed to mix the nanoclay with the asphalt binder. Rotational Viscosity (RV), Dynamic Shear Rheometer (DSR), Optical Contact Analyzer (OCA) and Atomic Force Microscope (AFM) were conducted to evaluate the properties of modified asphalt binders. Significant increases of viscosity and complex shear modulus were observed for nanoclay-modified binders because of nanoclay's nanoscale phenomena such as structural features, quantum effects, spatial confinement, high surface energy, and a large fraction of surface atoms. The maximum rutting resistance is expected for binders modified with the 1% Cloisite 11B. The OCA test results suggest that the modified asphalt binders possess higher surface free energy than the neat binder. Therefore, cohesive energy which is an indicator of moisture damage was increased for modified binders. From the AFM analysis, adhesion and deformation values decreased for modified asphalt binders. The minimum adhesion and deformation values were found for asphalt binder samples modified with the 1% Cloisite 10A.

17. Key Words	18. Distribution Statement
Nanoclays, Binder, Cloisite, Rutting, Stripping, SARA	No restrictions.

19. Security Classif. (of this report)	20. Security Classif. (of this page)	21. No. of Pages	22. Price
Unclassified	Unclassified	76	

Form DOT F 1700.7 (8-72) **Reproduction of completed page authorized.**

SI* (MODERN METRIC) CONVERSION FACTORS

APPROXIMATE CONVERSIONS TO SI UNITS

Symbol	When You Know	Multiply By	To Find	Symbol
		LENGTH		
in	inches	25.4	millimeters	mm
ft	feet	0.305	meters	m
yd	yards	0.914	meters	m
mi	miles	1.61	kilometers	km
		AREA		
in^2	square inches	645.2	square millimeters	mm^2
ft^2	square feet	0.093	square meters	m^2
yd^2	square yard	0.836	square meters	m^2
ac	acres	0.405	hectares	ha
mi^2	square miles	2.59	square kilometers	km^2
		VOLUME		
fl oz	fluid ounces	29.57	milliliters	mL
gal	gallons	3.785	liters	L
ft^3	cubic feet	0.028	cubic meters	m^3
yd^3	cubic yards	0.765	cubic meters	m^3
		NOTE: volumes greater than 1000 L shall be shown in m^3		
		MASS		
oz	ounces	28.35	grams	g
lb	pounds	0.454	kilograms	kg
T	short tons (2000 lb)	0.907	megagrams (or "metric ton")	Mg (or "t")
		TEMPERATURE (exact degrees)		
^oF	Fahrenheit	5 (F-32)/9 or (F-32)/1.8	Celsius	^oC
		ILLUMINATION		
fc	foot-candles	10.76	lux	lx
fl	foot-Lamberts	3.426	$candela/m^2$	cd/m^2
		FORCE and PRESSURE or STRESS		
lbf	poundforce	4.45	newtons	N
lbf/in^2	poundforce per square inch	6.89	kilopascals	kPa

APPROXIMATE CONVERSIONS FROM SI UNITS

Symbol	When You Know	Multiply By	To Find	Symbol
		LENGTH		
mm	millimeters	0.039	inches	in
m	meters	3.28	feet	ft
m	meters	1.09	yards	yd
km	kilometers	0.621	miles	mi
		AREA		
mm^2	square millimeters	0.0016	square inches	in^2
m^2	square meters	10.764	square feet	ft^2
m^2	square meters	1.195	square yards	yd^2
ha	hectares	2.47	acres	ac
km^2	square kilometers	0.386	square miles	mi^2
		VOLUME		
mL	milliliters	0.034	fluid ounces	fl oz
L	liters	0.264	gallons	gal
m^3	cubic meters	35.314	cubic feet	ft^3
m^3	cubic meters	1.307	cubic yards	yd^3
		MASS		
g	grams	0.035	ounces	oz
kg	kilograms	2.202	pounds	lb
Mg (or "t")	megagrams (or "metric ton")	1.103	short tons (2000 lb)	T
		TEMPERATURE (exact degrees)		
^oC	Celsius	1.8C+32	Fahrenheit	^oF
		ILLUMINATION		
lx	lux	0.0929	foot-candles	fc
cd/m^2	$candela/m^2$	0.2919	foot-Lamberts	fl
		FORCE and PRESSURE or STRESS		
N	newtons	0.225	poundforce	lbf
kPa	kilopascals	0.145	poundforce per square inch	lbf/in^2

TABLE OF CONTENTS

LIST OF FIGURES

LIST OF TABLES

ACRONYMS, ABBREVIATIONS, AND SYMBOLS

A	Viscosity Intercept
AAS	Arkansas Academy of Science
AASHTO	American Association of State Highway and Transportation Officials
AFM	Atomic Force Microscope
ASTM	American Society for Testing and Materials
CR	Compatibility Ratio
DSR	Dynamic Shear Rheometer
FHWA	Federal Highway Administration
G*	Complex Shear Modulus
NNI	National Nanotechnology Initiative
OCA	Optical Contact Analyzer
PFQNM™	Peak-Force Quantitative Nanomechanical Mapping
PG	Performance Grade
PMB	Polymer Modified Binders
RTFO	Rolling Thin Film Oven
RV	Rotational Viscosity
SBR	Styrene-Butadiene-Rubber
SBS	Styrene-Butadiene-Styrene
SEBS	Styrene-Ethylene–Butylene-Styrene
SFE	Surface Free Energy
VTS	Viscosity Temperature Susceptibility
δ	Phase Angle

EXECUTIVE SUMMARY

Nanoclays are minerals which have a high aspect ratio and with at least one dimension of the particle in the nanometer range. The main goal of this study is to assess the feasibility of the use of nanoclay as an alternative of commonly used polymers such as styrene-butadiene-styrene (SBS) to modify performance grade (PG) of asphalt binders. Unmodified PG 64-22 asphalt binders were collected from two different sources for this study. One source was Ergon at Memphis, TN, defined as Source 1 and another source was Marathon at Catlessburg, KY, defined as Source 2. Three different types of organically treated nanoclays, namely, Cloisite 10A, Cloisite 11B, and Cloisite 15A, were used. Nanoclays at 1%, 2% and 3% by weight of asphalt binder were selected for blending with unaged/fresh asphalt binders. After different trials of temperature, time and rotational speed, a blending protocol was developed. Nanoclays were then blended with the unaged asphalt binders using a high shear mixer. The viscosity of the control and nanoclay-modified asphalt binder were evaluated. Viscosity tests were conducted from 135^{o}C to 180^{o}C in 15^{o}C intervals. The viscosity values significantly increased for the nanoclay-modified binders compared to neat binders. The binder modified by nanoclay 2% Cloisite 10A showed the highest viscosity.

For characterizing the viscous and elastic behavior of the neat binder and blended asphalt, dynamic shear rheometer (DSR) tests were performed for both unaged and the rolling thin film oven (RTFO) aged binders. For both unaged and RTFO aged binders, the values of the dynamic shear modulus (G^*) were increased and the value of the phase angles (δ) were decreased for nanoclay-modified binders compared to the neat binders. Consequently, the rutting resistance ($G^*/\sin\delta$) was also increased for nanoclay-modified binders. The maximum rutting resistance was expected when the neat binder was modified by 1% nanoclay Cloisite 11B. It was also found that the nanoclay-modified asphalt binder was less susceptible to temperature compared to the neat binder.

An optical contact analyzer (OCA) was used to evaluate the moisture susceptibility of the nanoclay-modified binders and aggregates (gravel and sandstone). The sessile drop method was followed to estimate the surface free energy (SFE) and the compatibility ratio (CR) of the modified binder samples and aggregates. The contact angle, the angle between the solid-liquid interface which is a combined effect of cohesion, adhesion, and wettability, increased for nanoclay-modified asphalt binders. The SFE value which indicates the moisture resistance increased when Source 1 binder modified by nanoclay and decreased when Source 2 binder modified by nanoclay. Based on CR results, gravel was found to perform better than sandstone when the binders were modified with nanoclays. An atomic force microscope (AFM) was used to evaluate morphological and nanomechanical properties (e.g., modulus, deformation, and adhesion) of neat and modified asphalt binders. The surface roughness increased, but the deformation values were found to decrease for the modified asphalt binders. The adhesion value, which indicates the moisture susceptibility, of the nanoclay-modified binder, improved significantly compared to the neat binder.

IMPLEMENTATION STATEMENT

The research team has shared findings with Arkansas Department of Transportation (ARDOT) engineers at their annual research symposium held in May 2018. The research team also participated in various workshops and conferences and delivered oral and poster presentations. The research team also presented findings at the 2018 Tran-SET Conference, held on April 3-4, 2018 in New Orleans, LA, the 2018 Arkansas Academy of Science conference, held on April 5-6, 2018 in Jonesboro, AR, the 2018 Create@state Research Day Symposium, held on April 16-18, 2018 in Jonesboro, AR. Major publications based on the findings of the current study are listed below:

- Morshed, MMT., Hassan, M. N., and Hossain, Z. (2018). Use of Nanoclays as Alternatives of Polymers Toward Improving Performance of Asphalt Binders. 2018 Tran-SET Conference, April 3-4, 2018, New Orleans, LA.
- Hossain, Z., and Bairgi, B. (2018). Viability of the Use of Nanoclay-modified Asphalt Binders in Roofing Shingles, 2018 CRC Conference, New Orleans, April 3-4, 2018, New Orleans, LA.
- Morshed, MMT., and Hossain, Z. (2018). Viscosity Temperature Susceptibility Analysis for Nanoclay Modified Asphalt Binders. 2018 Create@state Research Day Symposium, held in April 2018 at Arkansas State University, Jonesboro, AR.
- Morshed, MMT., and Hossain, Z. (2018). Prospects of Nanoclay as a Pavement Construction Material. Arkansas Academy of Science 102nd Annual Meeting, held in April 2018 at Arkansas State University, Jonesboro, AR.

The research team plans to share the findings at upcoming technology transfer events such as the 2018 ASCE Chapter meeting and the 2018 Oklahoma Research Day. The graduate student will publish the findings in the form of a Master's thesis. The research team also plans to publish the findings of this study in other relevant transportation materials journals and symposiums.

1. INTRODUCTION

With the increase of traffic volume in recent years, there have been substantial increases in traffic loads and tire pressures upon the road pavements. A combination of extreme weather events and increased loads has been pointed out as the primary cause of the pavement's premature distresses such as rutting and cracking. Producers have come up with different asphalt modifiers for increasing rut resistance of asphalt at service temperatures as well as decreasing the stiffness at low temperatures to improve the asphalt resistance to thermal cracking. Among other polymers, styrene-butadiene-styrene (SBS) and styrene-butadiene-rubber (SBR) are widely being used to modify performance grade (PG) binders so that asphalt can sustain increased loads and extreme temperature events. In this study, nanoclay has been used as an alternative asphalt modifier.

Nanoclay is economical and naturally abundant. Moreover, it is expected that the use of nanoclay instead of polymers could significantly reduce the cost of asphalt binders. Nanoclays possess an extraordinary potential for improving the performance of asphalt binders and mixes due to their nanoscale phenomena such as the quantum effects, high surface energy, spatial confinement, and a large fraction of surface atoms. A significant portion of the current usages of polymer-modified binders (PMBs) can potentially be replaced by nanoclay-modified binders.

Nanoclays are layered silicates that are found naturally, and hence they are environmentally safe, economical, and sustainable. One of the most frequently used layered silicates is montmorillonite (MMT), which has a 2:1 layered structure with two silica tetrahedron layers sandwiching an alumina octahedron layer. These three layers together form one clay sheet that has a thickness of 0.96nm. Thus, the individual clay sheets are classified as nanomaterial. Though the application of nanoclays in asphalt pavements is relatively new, it has the potential to be used for improving the mechanical, thermal, and barrier properties.

1.1. Literature Review

Several publications were reviewed for gathering existing information on the nanoclays and their impact on asphalt or any other similar petroleum products. The primary objective of this literature review is to gather all the information from the previous researches so that all efforts can be focused on further exploration of nanoclay modification of asphalt binders. Journals from different reputed publications including Transportation Research Records, Federal Highway Administration (FHWA) records, and projects of departments of transportation (DOTs) were considered for the literature review. Most of the pavements in the United States is flexible asphalt pavement. This type of pavement requires high maintenance costs. Considering the amount required during construction (only about 5% by weight), the quality of the asphalt binder plays an influential role on the flexible pavement performance. Parameters like surface properties and temperature susceptibility characteristics of asphalt have impacts on asphalt mixes. That's why it is not new to try polymer additives with virgin binders for improved mechanical performance. Styrene-butadiene-styrene (SBS) has been considered for enhancing the mechanistic properties and functional characteristics, although it increases the overall cost of the binder *(1)*. In December of 2017, the price of unmodified PG 64-22 asphalt was $355.00 per ton. Whereas, the cost of a polymer-modified binder ranges from 50-100% more than the neat binder *(2)*. Per Arkansas department of transportation program management division, the price

per gallon of polymer-modified asphalt binders was $4.03 (approximately $1096.54 per ton) in 2017 *(3)*.

Many researchers (e.g., *(4)* and *(5)*) have claimed that when HMA mix is dispersed at a nanoscopic level, nanoclays improve the performance of asphalt binders due to their nanoscale phenomena including quantum effects, structural features, high surface energy, spatial confinement, and large fraction of surface atoms *(4,5)*. Moreover, nanoclays are cheaper than other modifiers as they are naturally abundant. So, nanoclays have the potential to replace the existing modifiers for improved mechanical and functional characteristics of asphalt pavements *(6)*.

Many researchers suggested different mixing protocols of nanoclay with asphalt binder. Most of the researchers used a high shear mixer for blending the nanoclay with the binder. You et al. *(4)* suggested a new blending protocol that used a rotation of 2500 rpm, a temperature of 160°C, and a mixing duration of 3 hours. They used X-ray diffraction (XRD) that indicates the nanoclay particles were uniformly dispersed within the modified mixture. Yao et al. *(7)* used another blending protocol that consists of a rotation of 4000 rpm, a temperature of 130°C, and a mixing duration of 2 hours. Zhang et al. *(8)* used two steps of mixing. At first, they mixed nanoclay with the binder at 160°C for 20 minutes at the rotation speed of 2000 rpm. Then, they increased the temperature to 170°C for 40 minutes with a rotational speed of 4500 rpm. Abdullah et al. *(9)* used a different blending protocol for different types of nanoclay. Melo and Triches *(10)* embedded using a high shear mixer with a rotation of 5000 rpm.

Structurally nanoclays are layered silicates which have 2:1 layered structure with two silica tetrahedron layers sandwiching an alumina octahedron layer *(11,12)*. Due to this large surface area and energy, nanoclays have the potential to improve the binder's physical, mechanical, and rheological properties like fracture toughness, moduli, strength, heat resistance, gas permeability, flammability, and biodegradability. You et al. *(4)* also studied the effect of multiple nanoclays on a specific asphalt binder (PG 58-34). The complex shear modulus (G*) increased 66% and 125% for 2% and 4% nanoclay modifications, respectively. Jahromi and Ahmadi *(13)* tried Cloisite 15A and Nanofill15 as an asphalt binder modifier and observed increased stiffness, rutting resistance, indirect tensile strength, and a resilient modulus but a decreased fatigue performance.

Many researchers have incorporated nanoparticles effectively in laboratory studies. Ghile *(14)* studied Cloisite and reported that nanoclay modification enhanced the mechanical properties such as creep and fatigue resistance. Nanoclay also works as filler reinforcements. Yu et al. *(15)* reported that montmorillonite modified asphalts had higher viscoelastic properties and rutting resistance. Polacco et al. *(16)* also examined the polymer-modified asphalts to find out the effect of the addition of clay. You et al. *(4)* studied two types of nanoclays (A and B) as modifiers of a performance grade binder PG 58-22 in Michigan and reported a significant increase of rutting resistance of nanoclay-modified binders. Jahromi and Khodaii *(13)* studied two types of nanoclays, namely, Cloisite 15A and Nanofill 15, and they also reported improved rutting resistance and stiffness of nanoclay-modified binders. Hossain et al. *(5)* evaluated the viscosity and rutting properties of Cloisite 15-modified asphalt binders. Zapién-Castillo et al. *(17)* investigated nanocomposite styrene-ethylene–butylene-styrene (SEBS) Cloisite 15A-modified asphalt binders and reported favorable test results.

The Superpave specifications for the performance of an asphalt binder mainly focus on its macro-scale workability, consistency and strength properties. An Atomic Force Microscope (AFM) can be used to evaluate such molecular level mechanistic properties, which can be used to predict the field performance of asphalt pavements *(18).*

An AFM works based on the van der Waals attraction force, which is the intermolecular residual attractive or repulsive forces other than those arise from a covalent bond or electrostatic interaction. The AFM can capture nanoscopic level data that provides the morphology of the surface of the asphalt binders as well as the nanomechanical properties such as elastic modulus, hardness, adhesion, and energy dissipation. Multiple studies *(19-21)* have estimated mechanical properties of asphalt binders using different AFM systems. Masson et al. *(21)* analyzed 13 asphalt binder samples to characterize the surface morphology, and they observed distinct morphological clusters, which were previously unseen or not reported by any other studies.

Recently, dispersed phase, interstitial phase, and matrix are more commonly used by researchers *(22-24)* to identify different phases instead of Catana, Peri-, and Para-phase. Dourado et al. *(20)* used the AFM-based nanoindentation technique to evaluate selective mechanical properties (e.g., elastic modulus) at different places on the surfaces of different asphalt binder samples. Yu et al. *(25)* developed a systematic AFM-based test procedure to evaluate the adhesive properties of asphalt binders and reported that the adhesion in the "raised areas" of the morphological image is twice of that in the recessed areas. Although the nanoindentation method was used in previous studies to calculate the modulus and adhesion properties of the asphalt binders, this method has some limitations regarding specific loading parameters *(26)*, the thickness of the testing material, difficulties in data acquisition *(27)*, and the time-consuming analysis process. A relatively new method, PeakForce Quantitative Nanomechanical Mapping (PFQNM™), was used for the similar purpose by Nahar et al. *(23)* and Fisher et al. *(24)*. The PFQNM™ method had many advantages over the nanoindentation method.

Surface free energy (SFE) analysis of asphalt is one of the science-based approaches that have received significant attention from the pavement professionals and researchers around the globe. The SFE approach is based on surface science approach, which overcomes the limitation of conventional test methods such as the Tensile Strength Ratio (TSR) or Hamburg Wheel Test Device (HWTD) method.

Some researchers at the Texas Transportation Institute (TTI) *(28,29)* introduced a parameter "compatibility ratio (CR)" in the surface free energy (SFE) theory. The CR is the ratio of work of adhesion of an aggregate and the binder system in dry condition to the adhesion of the same system in the presence of water. For evaluating the SFE of asphalt binders, researchers used the Good-van Oss-Chaudhury theory, in which the SFE is divided into three components based on their intermolecular forces: (1) monopolar acidic component (Γ^{+}), (2) monopolar basic component, (Γ^{-}), and (3) a polar or Lifshitz-van de Waals (Γ^{LW})] component. And, the total SFR for a single phase is divided into a Lifshitz-van der Waals component (Γ^{LW}) and an acid-base (AB) component (Γ^{AB}), which can be written as shown in Equation 1.

$$\Gamma^{total} = \Gamma^{LW} + \Gamma^{AB} \quad [1]$$

Where the acid-base part of the free energy can be described as shown in Equation 2.

$$\Gamma^{AB} = 2\sqrt{(\Gamma^{+}\Gamma^{-})} \quad [2]$$

The Gibb's free energy of adhesion (ΔGad) also consists of two components, as shown in Equation 3.

$$\Delta Gad = \Delta G^{LW}_{ad} + \Delta G^{AB}_{ad} \quad [3]$$

The individual components of Equation 3 are given by Equations 4 and 5.

$$\Delta G^{AB}_{ad} = -2\{\sqrt{(\Gamma^{+}_{i}\Gamma^{-}_{j})} + (\sqrt{(\Gamma^{-}_{i}\Gamma^{+}_{j})}\} \quad [4]$$

$$\Delta G^{LW}_{ad} = = -2\sqrt{(\Gamma^{LW}_{i}\Gamma^{LW}_{j})} \quad [5]$$

Combining these equations, the Young-Dupre equation for the work of adhesion can be found, as shown in Equation 6.

$$W^{a} = -\Delta G^{ad}_{dry} = \Gamma^{total}_{L}(1+\cos\theta) = 2\{\sqrt{(\Gamma^{LW}_{L}\Gamma^{LW}_{S})} + \sqrt{(\Gamma^{+}_{L}\Gamma^{L-}_{S})} + \sqrt{(\Gamma^{-}_{L}\Gamma^{+}_{S})} \quad [6]$$

Where the L and S denote liquid and solid, respectively. This equation was used for further calculation of the SFE components of the asphalt binder with reference solvent by evaluating the contact angles using the modified asphalt binders. For measuring the three unknown free energy components of the asphalt binder, three reference solvents have been recommended by many researchers (Bhasin A. et al., 2006). In a similar way, the free energy of adhesion between the asphalt binder and aggregate in the presence of water is expressed as shown in Equation 7.

$$\Delta G^{ad}_{wet} = 2\Gamma^{LW}_{w} + 2\sqrt{(\Gamma^{LW}_{a}\Gamma^{LW}_{A})} - 2\sqrt{(\Gamma^{LW}_{a}\Gamma^{LW}_{w})} - 2\sqrt{(\Gamma^{LW}_{A}\Gamma^{LW}_{w})} + 4\sqrt{(\Gamma^{+}_{w}\Gamma^{-}_{w})} + 2\sqrt{(\Gamma^{+}_{a}\Gamma^{-}_{A})} - 2\sqrt{(\Gamma^{-}_{a}\Gamma^{+}_{A})} + 2\sqrt{(\Gamma^{+}_{a}\Gamma^{-}_{w})} - 2\sqrt{(\Gamma^{-}_{a}\Gamma^{+}_{w})} - 2\sqrt{(\Gamma^{+}_{A}\Gamma^{-}_{w})} \quad [7]$$

The free energy cohesion (ΔG_c), which is the creation of a unit area of crack within a material in a vacuum condition, can be determined by using Equation 8.

$$\Delta G_c = 2\Gamma^{total} \quad [8]$$

The effect of different additives on the cohesive strength and adhesive strength between asphalt binders and aggregates has also been studied by many researchers (e.g., *22, 26*). From these studies, it can be implicated that the SFE and other surface properties depend on various factors such as the type of asphalt binder, type of aggregate, and type of additive used.

2. OBJECTIVES

The primary objective of the proposed study is to assess the feasibility of using nanoclays as modifiers of base asphalt binders. Specific objectives of the proposed study are to:

- Develop a suitable blending protocol to modify base asphalt binders with nanoclay; and
- Examine performance properties (rutting, fatigue, and moisture resistance) of nanoclay-modified asphalt binders.

To fulfill the objectives of the project, the following tasks have been identified:

- Collect required asphalt binders and nanoclays required for this research;
- Blend nanoclays with selective base asphalt binders using a high shear mixer and examine their dispersion properties toward developing a suitable protocol. Investigate the effect of size, surface modification and dosages of nanoclays on critical properties of the asphalt binder;
- Evaluate the role of nanoclays in altering the rheological properties of the asphalt binder;
- Study the effect of nanoclays on aging properties of the asphalt binder;
- Evaluate moisture susceptibility of the modified binders;
- Perform chemical analysis of nanoclay-modified binders; and
- Conduct life cycle cost analysis of different nanoclay-modified asphalt binders.

3. SCOPE

Neat binders are usually modified by SBS and SBR to sustain increased load and extreme temperature events. Such modifications increase the overall cost of the binder. Alternatively, nanoclay is economical and naturally abundant. It is expected that the use of nanoclay instead of polymers will significantly reduce the cost of asphalt binders. However, the transportation agencies do not have sufficient performance data of nanoclay-modified asphalts. Thus, this study has attempted to gather performance data of nanoclay-modified asphalt binders. This experimental study is limited to the literature review and laboratory investigation of asphalt binders modified with commercial nanoclays. Besides Superpave tests and selective chemical tests, surface free energy (SFE) measurements and atomic force microscopy (AFM) analysis were undertaken. The chemical tests included SARA analysis and FTIR spectroscopy. Finally, a life cycle cost analysis has been performed to determine economic benefits of nanoclay-modified binders compared to polymer-modified binders.

4. METHODOLOGY

4.1. Material Selection

Two virgin PG 64-22 binder samples were collected from Ergon Inc. which was an industry partner for this study. One sample originated from a Canadian crude source, and the other binder sample was made from an Arabian crude source. Three types of organically treated nanoclay were used to modify the virgin binders: Cloisite 10A, Cloisite 11B, and Cloisite 15A. The virgin binders were modified using three different percentages of modifiers: 1%, 2%, and 3%. These nanoclays were collected from Southern Clay Products, Inc. Cloisite 15A and Cloisite 10A share very similar plate dimension (~13 microns), but they were treated with different types of modifiers. Cloisite 15A was modified with dimethyl, dihydrogenerated tallow, and quaternary ammonium salt. On the other hand, Cloisite 10A and Cloisite 11B were modified with a dimethyl, benzyl, hudrogenerated tallow, and quaternary ammonium salt. The average plate dimensions for Cloisite 10 A and Cloisite 11B are 13 and 37-microns, respectively. Table 1 summarizes the details of the nanoclay systems used in the project. Both the effect of nanoclay size and type on the characteristics of nanoclay-modified asphalt binder were investigated during the project. To be more specific, mechanistic properties, including stiffness, strength resistance, and moisture barrier characteristics were considered for performance evaluation of nanoclay-modified binders. There was also an effort to find out an optimum percentage of nanoclay for modification in this study. The percentages of nanoclay (1%, 2%, and 3%) were selected based on existing literature and manufacturer's recommendations.

Table 1. Nanoclay properties.

Properties	Nanoclay 1 (Cloisite 15A)	Nanoclay 2 (Cloisite 10A)	Nanoclay 3 (Cloisite 11B)
Organic Modifier	2M2HT	2MBHT	2MBHT
Average Particle Size	13	13	37
Density (g/cc)	1.66	1.9	2.0
Inter-gallery Spacing (Angstrom)	31.5	19.2	18.4

4.2. Blending Protocol of Nanoclays and Asphalt Binder

A high shear mixer was used to blend the nanoclay with asphalt binder. The high shear mixer (Figure 1) can be operated at different durations, rotational speeds, and temperatures. Nine different trials were conducted using different times (2h, 3h, and 4h), rpm (1500 and 2000) and temperatures (150℃ and 160℃). Rotational Viscosity (RV) test, Dynamic Shear Rheometer (DSR) test, and Atomic Force Microscope (AFM) tests were completed for each trial. From the DSR test, complex shear modulus and phase angle were calculated. The $G^*/\sin\delta$ results versus temperature were plotted. From the AFM test, the morphology, adhesion, DMT modulus, and deformation values of the samples were observed and compared for establishing the blending protocol.

Figure 1. High shear mixer.

4.3. Rotational Viscosity (RV) Test

A DV-II+ Pro rotational viscometer (Figure 2), manufactured by Brookfield Engineering Inc., was used to determine the viscosity of asphalt binders in the high-temperature range (135°C to 180°C) following AASHTO T 316 *(Ref)*. This test helped to determine the mixing and compaction of the nanoclay-modified asphalt binders. The RV test considered the torque required to maintain a constant rotational speed of a cylindrical spindle submerged in an asphalt binder sample at a constant temperature. The equivalent viscosity of this torque was given as the output in the rotational viscometer.

For RV testing, the asphalt binder was heated to obtain a certain fluidity. An approximately 10-gm sample was poured into the sample chamber. The chamber temperatures were set at different levels, 135°C to 180°C at 15°C increments, for measuring the viscosity of the asphalt binder sample. When the test temperature had reached the desired level, a time of 10 minutes was allowed for ensuring the stability of the chamber temperature. Then, the device was turned on and three separate readings were recorded at intervals of 1 minute. As per Superpave specifications, the rotational viscosity for an unaged asphalt binder should be no more than 3 Pa.s at 135°C. The viscosity data obtained at three different temperatures for the unaged binders were analyzed for determining mixing and compaction temperatures.

Figure 2. Rotational viscometer.

4.4. Rolling Thin Film Oven (RTFO) Aging

The nanoclay-modified asphalt binders were aged by using a rolling thin film oven (RTFO) to simulate the short-term aging (Figure 3). The aging procedures were performed in accordance with AASHTO T 240 *(Ref)*. The short-term aged samples were prepared for further testing as well as for simulating the long-term aging. At first, modified asphalt binders were heated so that the samples become fluid enough to pour into the RTFO bottles. Approximately 35 ± 0.5 g sample was taken from each modified binder and poured into the RTFO bottle. The bottles were properly labeled. The heating chamber of the RTFO was preheated at 163±1°C. After the preheating was completed, the bottles were mounted on the sample rack inside the hot chamber for aging purpose. The door was properly locked to reduce the heat loss as much as possible. The rotation speed of the sample rack was set at 15 rpm and the rate of air flow was 4 liters/min that was blowing directly into the bottles containing the asphalt binders. The aging operation continued for 85 minutes. It was the combination of airflow and heat that facilitated the oxidation of the asphalt binder. This oxidation consequentially simulated the short-term aging of asphalt binder. After 85 minutes of rotation in the combination of heat and airflow, the RTFO was turned off. The hot samples were then taken out of the bottles with a scraping tool and stored for further tests and PAV-aging.

Figure 3. Rolling thin film oven.

4.5. Pressure Aging Vessel (PAV) Aging

Pressure Aging Vessel (PAV) aging was done to simulate the long-term aging of the nanoclay-modified asphalt samples (Figure 4). As asphalt binders remain exposed to the weather throughout entire service life, experiences a longer oxidation period which causes long-term aging. PAV aging can simulate about 7-10 years of field aging. Long-term aging makes a binder stiffer and more susceptible to low-temperature cracking. This is the reason when evaluating the performance of nanoclay-modified binders, the RTFO modified samples were taken under long-term aging with PAV following the specifications of AASHTO R 28 *(Ref)*. At first, the temperature was set at 100°C for running the entire aging process. After reaching the anticipated temperature, the RTFO aged samples were placed in a pan, which was later placed into the specially designed vertical rack and then placed inside the PV chamber for long-term aging. The air pressure was set at 2.10 MPa which was supplied from the outside cylinder. After achieving the required combination of temperature and pressure, aging continued for approximately 20 hours. After the PAV aging, the chamber was depressurized, and the aged samples were taken out of the chamber and stored for further chemical and mechanical testing.

Figure 4. Pressure aging vessel (PAV).

4.6. Dynamic Shear Rheometer (DSR)

Dynamic Shear Rheometer tests were conducted on all nanoclay-modified asphalt binders for characterizing their viscoelastic properties (Figure 5 and 6). In this test method, two specific properties of a sample were tested: complex shear modulus (G*), which represents the total resistance offered by the asphalt binder under repeated shear loading, and phase angle, (δ), which represents the delay in the resulting shearing strain in an asphalt binder specimen in response to an applied shear stress. The Superpave rutting and fatigue factors depend on these parameters. This test was conducted by following the AASHTO T 315 method *(Ref)*. Asphalt binders were sandwiched between two parallel plates geometry. Then shearing stress was applied on the asphalt binder at a loading rate of 10 rad/sec (corresponding to 55 mph vehicle speed). For 25-mm diameter, parallel plates the intermediate gap was 1.00 mm. For 8.00-mm diameter plates, the gap was 2.00 mm. The Superpave specifications for the rutting and fatigue factors are presented in Table 2.

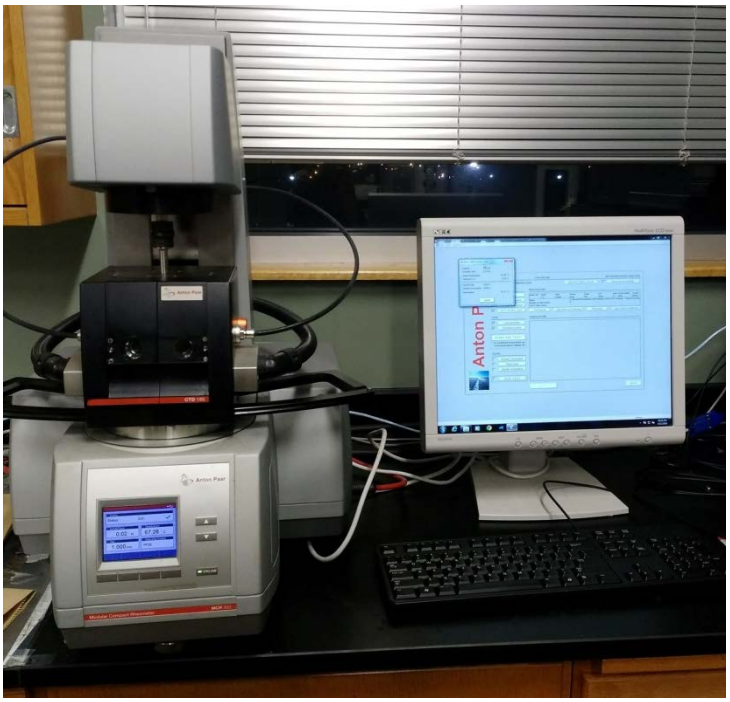

Figure 5. Dynamic shear rheometer (DSR).

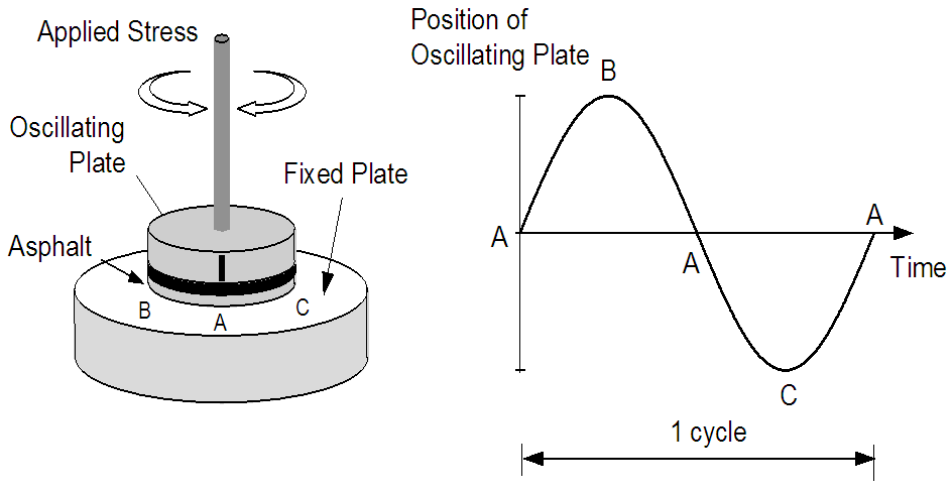

Figure 6. Dynamic shear rheometer setup.

Table 2. Superpave specifications for DSR test.

Binder Sample	Value	Test Temperature (°C)	Specification
Unaged binder	G*/sinδ	High Service	≥ 1.00 kPa (0.145 psi)
RTFO-aged binder	G*/sinδ	High Service	≥ 2.20 kPa (0.319 psi)
PAV-aged binder	G*.sinδ	Intermediate Service	≤ 5000 kPa (725 psi)

4.7. Sessile Drop

An optical Contact Analyzer (OCA) was used to evaluate the moisture susceptibility of the nanoclay-modified binders. The sessile drop method was followed to estimate the SFE and CR of the modified binder samples. In this method, a droplet of a liquid with known surface energy was placed on a solid surface. The shape of the drop, contact angle, and surface energy of the liquid could be used to determine the surface energy of the solid. Moisture susceptibility could be estimated from the change in surface free energy. Moreover, the observation of the CR values of the selected binder-aggregate system contributed to deciding the suitable aggregates for a specific type of modified binder. For conducting the required tests, an OCA 15 device (Figure 7) from Future Digital Scientific was used along with three reference solvents: water, ethylene glycol, and formamide.

In the Sessile drop experiment, static contact angles of asphalt binders for three reference liquids were measured, and the shape of the drop was analyzed by using the software connected to the OCA device (Figure 8). For one drop, more than 100 contact angles on each side of the drop were measured in this technique to get a very precise measurement. The volume of the drop was regulated, and the same drop volume was used for all the samples.

For determining the contact angle of the asphalt binder, a very smooth and thin surface of asphalt was created on a thin glass slide. At first, the asphalt binders were heated at a temperature of 163°C until they were fluid enough to spread over a solid surface. A glass slide of 57 mm x 70 mm x 1.5 mm was wrapped on all four sides with scotch tape to the desired sample outline. The glass slide was cleansed by quickly run through a flame before coating with the tape for ensuring it was free from any particles or charges. With the help of a trimmer, a very small amount of asphalt binder was placed over one of the sides of the taped area. Another glass slide was quickly pressed and slid over the taped area of the asphalt drop to spread the asphalt binder evenly and smoothly over the surface of the glass slide.

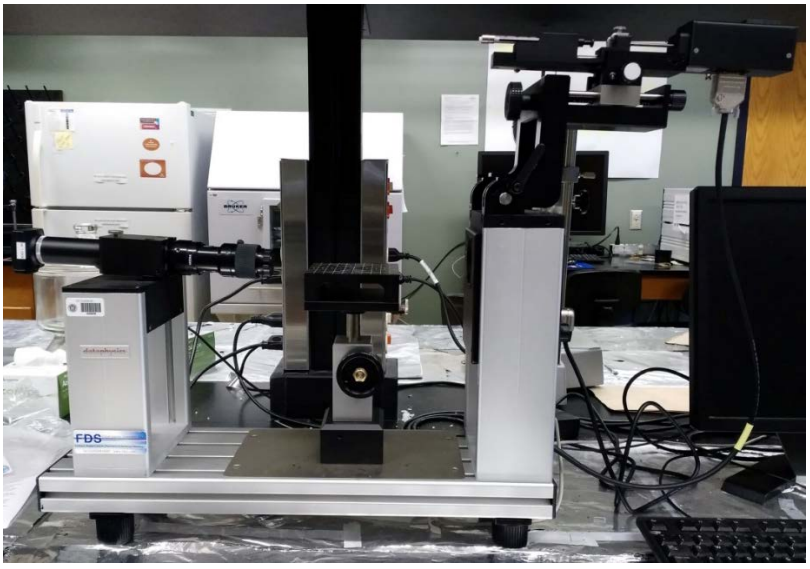

Figure 7. Optical contact analyzer (OCA).

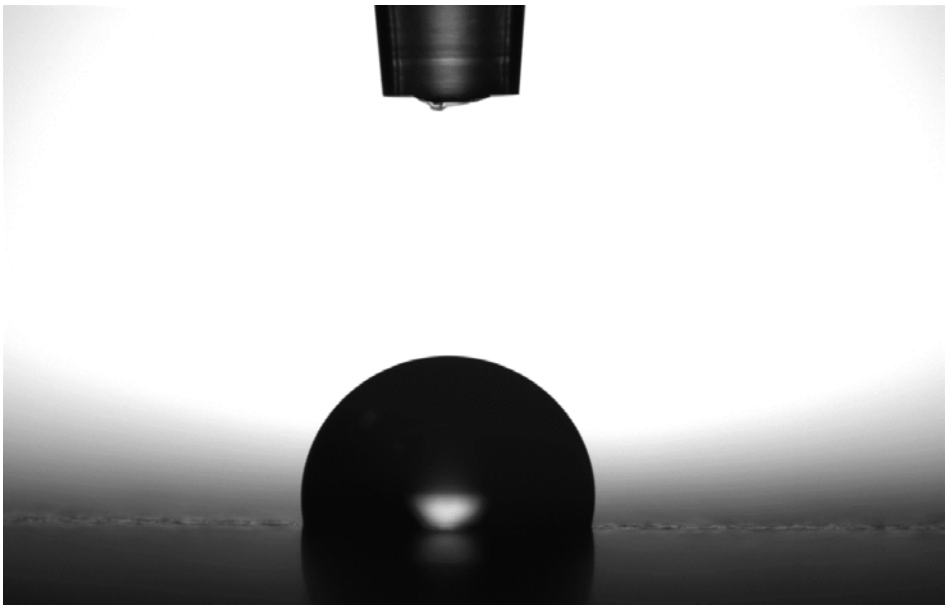

Figure 8. Sessile drop measurement with a contact angle analyzer.

4.8. Atomic Force Microscope (AFM)

Atomic Force Microscope (AFM) is also used by many researchers for evaluating moisture susceptibility. The AFM is a scanning probe microscope that can measure local properties like height, friction, magnetism with the help of a probe. This device raster-scans over a small area of the samples and measures the local properties and store them as images. It uses molecular properties to characterize the morphological and nanomechanical properties of the nanoclay-modified asphalt binders. The results from the AFM analysis were later compared with the sessile drop analysis to evaluate the nanoclay-modified asphalt binders.

A Dimension Icon AFM, manufactured by, Bruker (Figure 9), was used to investigate the surface morphology and nanomechanical properties of the nanoclay-modified asphalt binders. During the project, the Peak-Force Quantitative Nanomechanical Mapping (PFQNM™) mode of the AFM was used to observe the properties of the nanoclay-modified asphalt binders. For preparing the samples, the heat cast approach (HCA) was followed because it provides a natural surface of the asphalt. In the HCA, a small amount of nanoclay-modified binder was placed on a 50.8 mm x 76.2 mm glass plate. Then, the glass plate was placed in an oven at 160°C for approximately 15 minutes. A uniform and smooth surface of the asphalt binders was developed over the thin glass plate during the time of heating. The prepared samples were considered as “Dry Specimens” and were stored in a humidity-controlled desiccator. The samples were tested after three days. Prepared samples were then tested using the AFM.

Figure 9. Atomic force microscope.

4.9. SARA (Saturates, Aromatics, Resins, and Asphaltene) Analysis

A larger part of the chemical analysis of this project was composed of SARA analyses of asphalt binders. All the nanoclay-modified asphalt binders were characterized in terms of the changes in their chemical compositions. The SARA analysis is an acronym for the chemical constituents of the asphalt binders: Saturate, Aromatic, Resin, and Asphaltene. The test was executed in accordance with ASTM D 4124-09: Standard Test Method for Separating Asphalt into Four Fractions (*31*). The fundamental principle of this test was "like dissolves like." This principle implied that every constituent fraction had a certain degree of polarity for which it could only be moved with a solvent of similar polarity. The entire process was conducted through a sequential application of specific solvents and evaporating them to acquire the constituent fractions. The standard procedure was applied with a small adaptation in the laboratory.

Figure 10. Sample preparation.

For the SARA analysis, the asphalt sample was put inside an oven to facilitate sufficient fluidity so that it could be poured. As per the standard, the asphalt sample could also be alternatively collected by chilling to facilitate fracturing the sample. For heating the asphalt binder sample, the oven temperature was carefully maintained so that it did not exceed more than 50°C above the anticipated softening point, which was 100°C for the asphalt binders. Heating to higher temperatures could cause unexpected aging in the asphalt binder sample. After reaching the sufficient fluidity, the asphalt binder was poured into a tared round-bottomed flask (neck size 24/40) for sample preparation (Figure 10). An approximately 2.00±0.30 g sample was taken in for the refluxing operation.

The sample was then allowed to cool to the room temperature. Then, n-Heptane was added to the round-bottomed flask at a ratio of 100 mL for each gram of the sample. A stirring magnet was added into the round bottom flask to ensure the proper mixing of asphalt binder sample into n-heptane solvent. A Liebig condenser was required to fit with the neck of the round-bottomed flask. The opening of the Liebig condenser had to be compatible with a round-bottomed flask of 24/40 neck. The flask was then fastened with a clamp stand and put in a heating bath containing sand. The particle size of the sand had to be minus US standard sieve No. 20 (0.841 mm) and it was very important for ensuring an ease in dipping the round-bottomed flask into the bath.

The entire setup was arranged inside a fume hood. The hot plate/heating bath was turned on, and the temperature was set at 250°C. The stirring (at 350±50 rpm) had to be started once the sample started refluxing. During the heating, all the n-Heptane that could go upward due to the heat would come back because of the condenser. Thus, the temperature inside the round bottom flask could be maintained at the boiling point of n-Heptane (i.e. 98.42°C). The stirring action would be continued for 1 to 2 hours until no visual evidence of undissolved asphalt binder adhered to the flask. Once the entire sample was dissolved into the solution, stirring was continued for an additional 1 hour. Normally, 2 hours is sufficient for the complete dissolution, but for air blown asphalt or chemically-modified asphalt, the standard recommends extending the stirring time to 3 hours. After the refluxing operation, the heater was turned off, and the solution could cool down to the room temperature with the stirring action on. The stirring action was continued for an additional 2 hours after cooling. After the cooling process, the condenser was removed, and the solution could settle for 2 hours prior to the filtering operation.

Figure 11. Asphaltene separation.

A Buchner-style fritted glass funnel of medium porosity (ASTM 10-15 micrometer) was used for the filtering operation which separated the Asphaltene from the Maltene within the solvent (Figure 11). The refluxed asphalt sample was poured in and filtered through this funnel to separate the Asphaltene. The Asphaltenes are the solid fraction that could not pass through the porous disc on the funnel. Any solid residue that could not pass through at first trials were washed later with n-Heptane and poured again into the funnel. Suction was applied to a filtering flask to acceleration. Applying suction was important especially in cases of highly-aged or highly-modified binders where the filtering was much slower due to higher Asphaltene content. After the filtering was completed, the filter was weighed again to measure the accumulated the Asphaltene content.

The collected liquid in the filtering flask was the Maltene containing the Saturate, Aromatic, and Resin fractions. A column of activated alumina was required for separating the Maltene fractions. The glass column was dried completely before any experimental use. The activated alumina was poured in and filled up to the bottom of the spherical top. A cotton plug was inserted on top of the filled alumina. The column was ensured to be totally vertical as the chromatography was assisted by the gravity. A tilted gesture could have affected the fraction reaching the bottom in an uneven manner and would have yielded a mixed elution. The column was wetted with a little n-Heptane prior to loading the Maltene onto it. The bottom valve was kept open and a conical flask was fitted underneath to collect the elution.

Figure 12. Column chromatography.

The first elution from the column chromatography was the Saturates that came with n-Heptane (Figure 12). Once the liquid in the top spherical portion got depleted upon complete adsorption on the column, toluene was added, and it initiated the movement of the Aromatics fraction. The movement of the Aromatics fraction could be traced by shining a UV light (365 nm) on the column. A fluorescent band could be seen moving downward leaving the black portion back. The fluorescent band was the Aromatics portion of the whole asphalt binder. The fluorescent band

helped to pinpoint the start and cutoff points for the collection of the Aromatics from Saturates and Resins. Once the toluene depleted in the top sphere, a 50:50 mixture of toluene and methanol was introduced on top. It initiated the movement of the Resins fractions. The movement of the fluorescent band was carefully observed to start collecting the Resins dissolved in trichloroethylene. The ultraviolet (UV) detector was shined for just a little while to avoid causing any unexpected UV-aging to the binder.

The collected fractions were taken to a rotary evaporator for solvent-removal. The eluted fractions were not allowed to dry voluntarily as the solvents do not evaporate entirely through voluntary evaporation. Each eluted fraction was taken into separate round-bottomed flasks (Figure 13).

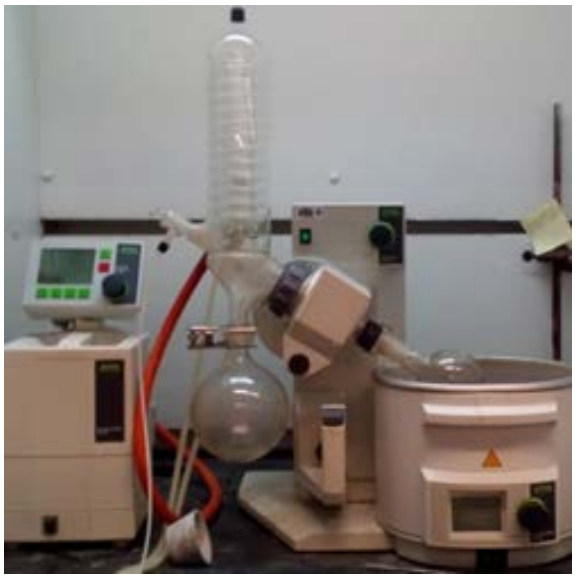

Figure 13. Evaporation of solvents.

The rotary evaporator lowered the atmospheric pressure inside the flasks through a vacuum pump and applied heat simultaneously. After a certain time, the solvent evaporation initiated. The temperature bath was kept constant at 79°C. The vacuum was applied gradually in a steady manner until the final set-point was achieved. For the Saturates dissolved in n-Heptane, the final pressure set-point was approximately 300±20 mbar. For the Aromatics dissolved in toluene, the pressure required approximately 200±20 mbar. For the Resins fractions dissolved in trichloroethylene, the pressure was set initially at 820 mbar and then gradually lowered down to 200 mbar. The pressure was reduced in situations when there was no visual sign of evaporation happening. In every case, chloroform was added to remove any remaining solvent. The freed fractions were dried in an oven overnight for obtaining a stable and precise mass.

Figure 14. Separated SARA fractions.

The separated fractions (Figure 14) were recorded for their dried masses and expressed as $M_{Saturates}$, $M_{Aromatics}$, *and* M_{Resins} for the Saturates, Aromatics, and Resins fractions, respectively. The masses were expressed as percent fractions of the original sample that was taken. About 90~99 % of the whole sample could be recovered through this column chromatography technique (Figure 15).

Figure 15. SARA fractions stored.

5. FINDINGS

5.1. Blending Protocol

As mentioned earlier, nanoclays were blended with the unaged asphalt binders using a high shear mixer. Nine different trials were conducted using different times (2h, 3h, and 4h), rotations (1500 and 2000), and temperatures (150°C and 160°C). RV, DSR, and AFM tests were completed for each trial. The naming convention can be seen in Appendix A of this report. The dynamic viscosity was determined at 135°C (Figure 16) and 150°C (Figure 17) with the help of the rotational viscometer. The viscosity for 2000 rpm, 150°C, and 2 hours have a very little variation with respect to time at a constant temperature compared to other trials (Figures 16 and 17). From the DSR test, complex shear modulus and phase angle were calculated. The rutting factor (G*/sinδ) versus temperature charts were plotted (Figure 18). Rotation 2000 rpm, temperature 150°C, and blending time of 2 hours were selected because (G*/sinδ) value is in an acceptable range and have a very little variation with respect to temperature. Other trials have higher (G*/sinδ) values but these may be happened due to the aging effect. From AFM test, the morphology, adhesion, DMT modulus, and deformation values (Table 3) of the samples were observed and compared. For a rotation of 2000 rpm, a temperature of 150°C, and a blending time of 2 hours. The surface morphology and deformation values were nearly the same compared to the neat binder. From the output of these tests, a blending protocol (2h time, 2000 rpm, and 150°C) was established to mix nanoclays with asphalt binders.

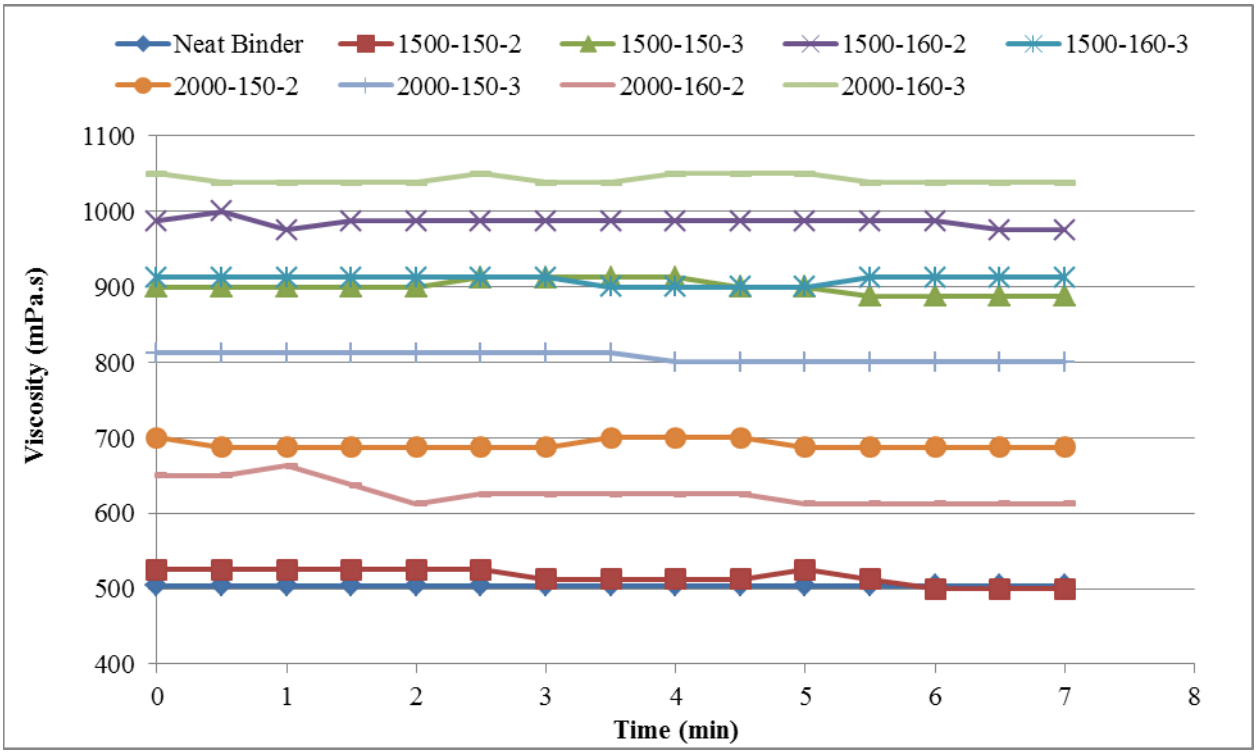

Figure 16. Viscosity (mPa.s) vs. time (min) curve at temperature 135°C for modified binders.

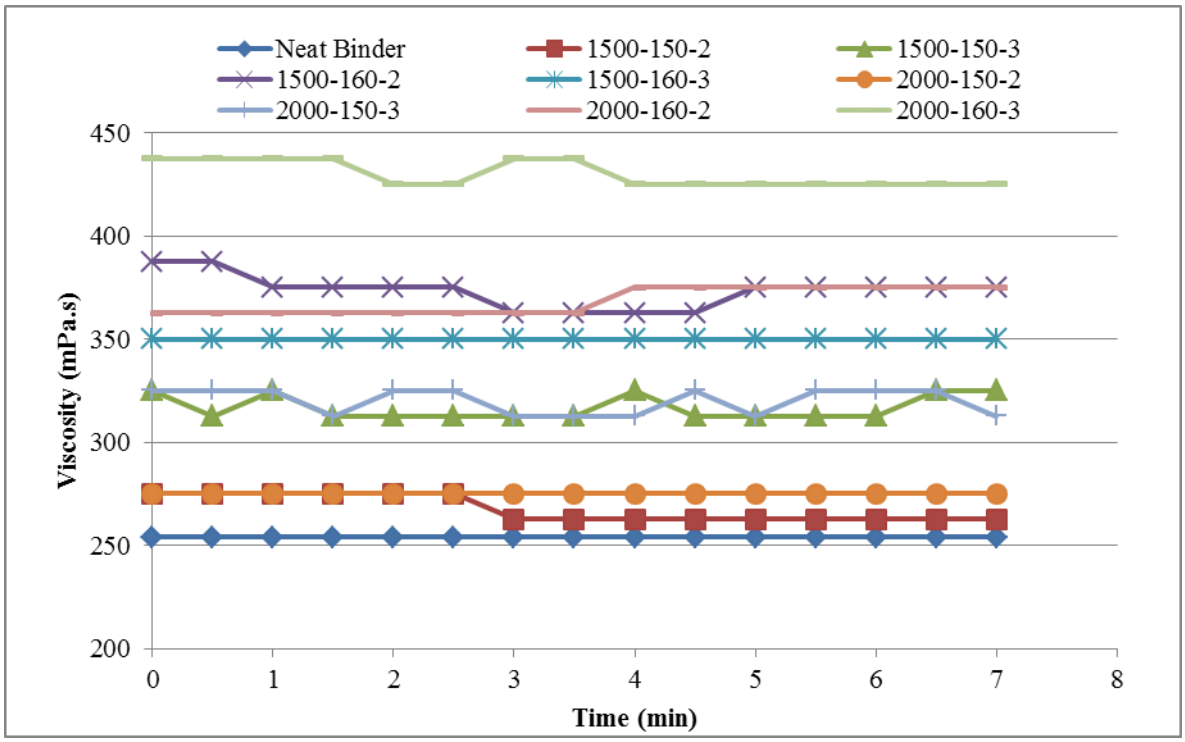

Figure 17. Viscosity (mPa.s) vs. time (min) curve at temperature 150°C for modified binders.

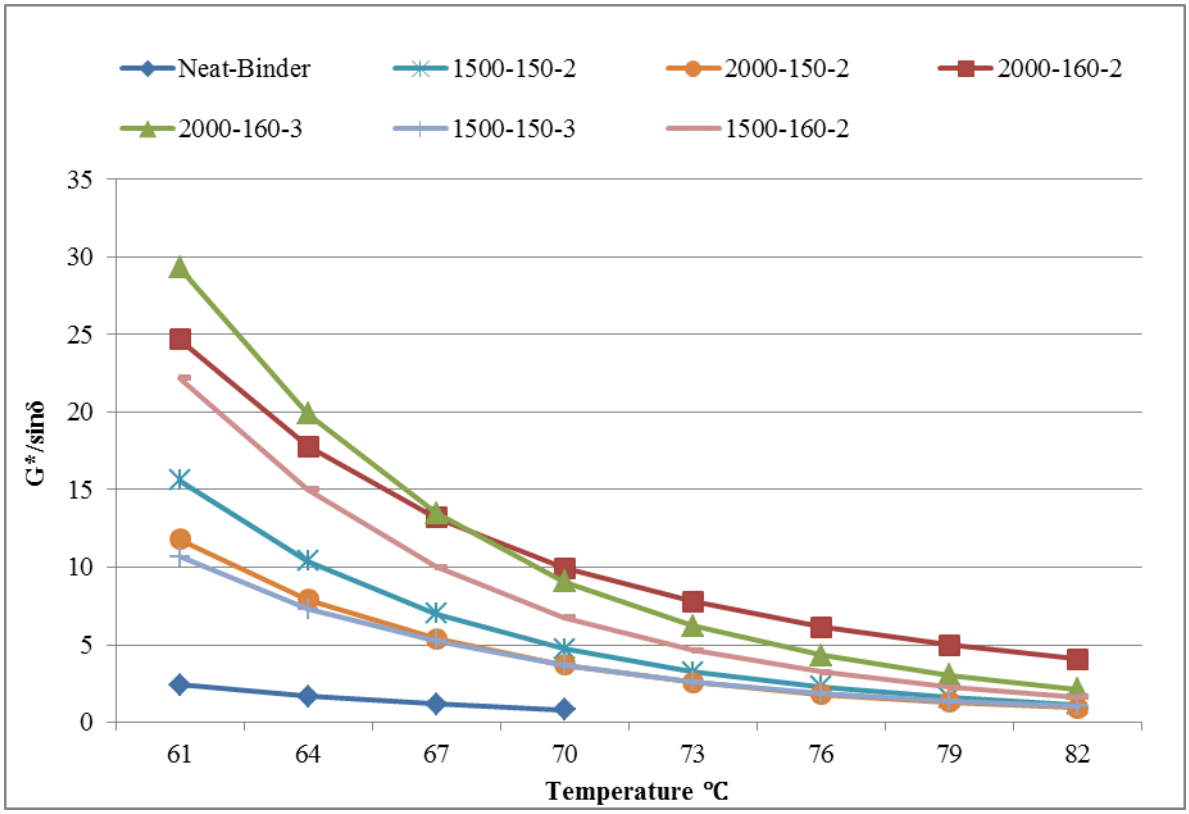

Figure 18. Rutting resistance (G*/sinδ) vs. temperature (°C) for modified binders.

Table 3. Value of the morphological and nanomechanical properties.

Sample Name	Surface Morphology (nm)	DMT Modulus (MPa)	Adhesion (nN)	Deformation (nm)
Neat Binder	5.36	122	20.5	3.19
1500-150-2	9.14	305	17.9	22.3
1500-150-3	5.31	178	21.2	4.55
1500-160-2	5.32	251	37.4	4.09
1500-160-3	6.13	152	20.2	3.25
2000-150-2	4.81	124	19.1	2.93
2000-150-3	5.15	156	28.4	3.81
2000-160-2	5.23	115	14.8	3.09
2000-160-3	12.6	122	17.6	3.09

5.2. Rotational Viscosity

For Source 2 (Marathon at Catlessburg) PG 64-22 binder modified by nanoclays, the viscosity values were also increased. For 1%, 2%, and 3% Cloisite 10A blended with asphalt binders, the viscosity values at 135°C increased by 187%, 140%, and 178%, respectively. At the same temperature, there were 162%, 162%, and 159% increase in viscosity when 1%, 2% and 3% Cloisite 11B was mixed with the Source 1 neat binder, respectively. For 1%, 2%, and 3% Cloisite 15A modified binders, viscosity values were increased by 102%, 111% and 114%, respectively at 135°C. Please see Appendix B for detail results of the RV tests.

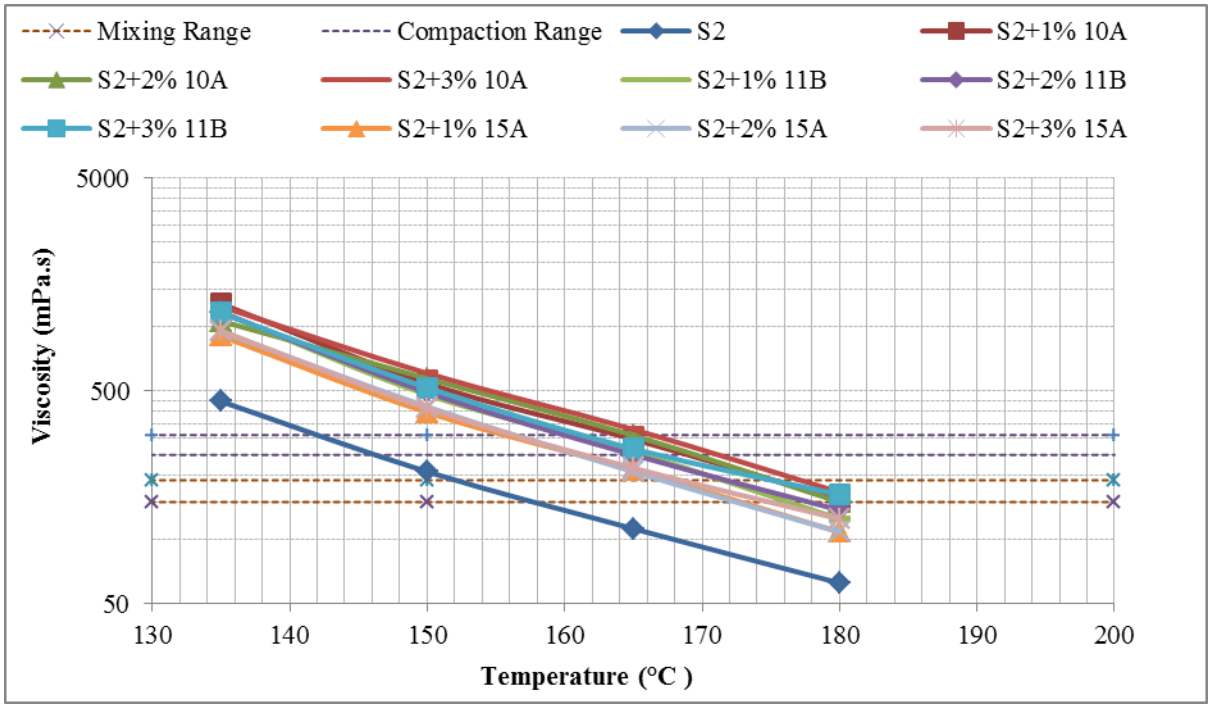

Figure 19. Viscosity (mPa.s) vs temperature (°C) curve for Source 2 modified binder.

5.3. Dynamic Shear Rheometer (DSR)

The G* (in log scale) versus δ, known as the black curve, was plotted in Figure 18. It is observed that the black curves for modified asphalt binders have shifted from the position of the neat binder to left. The G* values for nanoclay-modified asphalt binders increased and δ values decreased with respect to those of the neat asphalt binder. At 64°C, the maximum G* and the minimum δ are found when the asphalt binder was blended with the 1% Cloisite 11B. The "A" value (viscosity parameter) for nanoclay-modified asphalt binder is decreased from that of the neat binder. The absolute value of another viscosity parameter (VTS) is also decreased from that of the neat binder. Therefore, the nanoclay-modified asphalt binder is less temperature susceptible compared to the neat binder. Rutting factor (G*/sinδ) was also increased for modified binders and maximum rutting resistance was observed for binder modified with the 1% Cloisite 11B.

For Source 2 binder modified with nanoclays, the G* values for nanoclay-modified asphalt binders increased, and δ values decreased with respect to those of the neat asphalt binder. Maximum G* values were found when nanoclay 1% Cloisite 10A mixed with a neat binder. Detail results of DSR test can be seen in Appendix C.

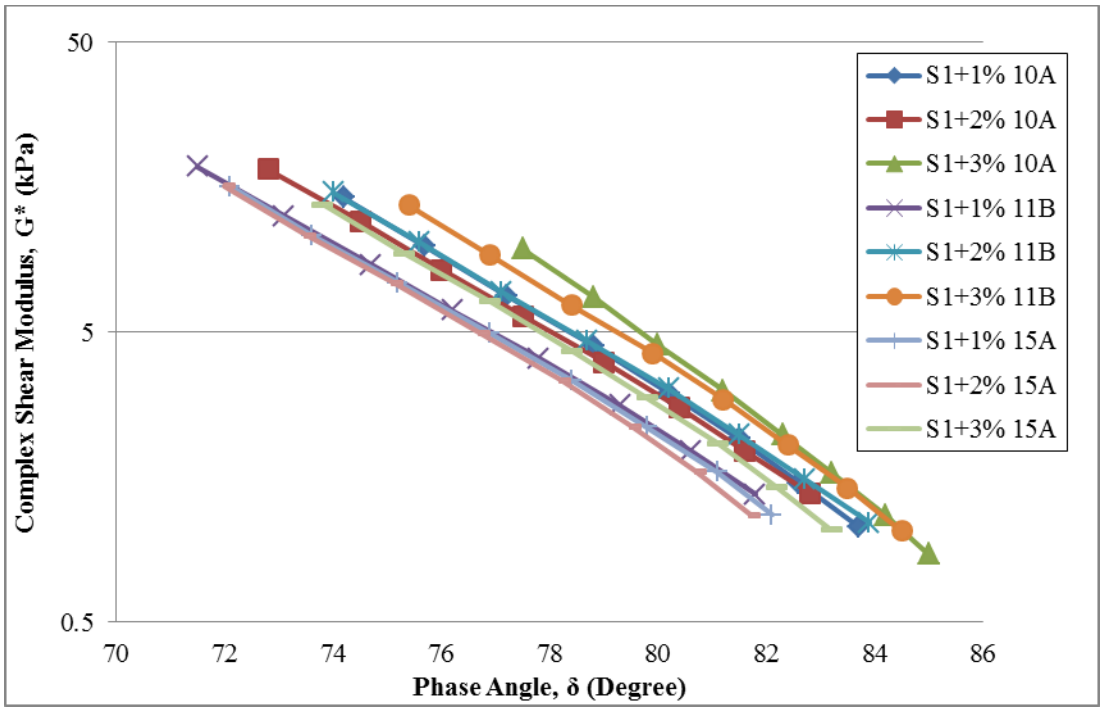

Figure 20. Complex shear modulus (G*) vs. phase angle (δ) curve for Source 1 modified binder.

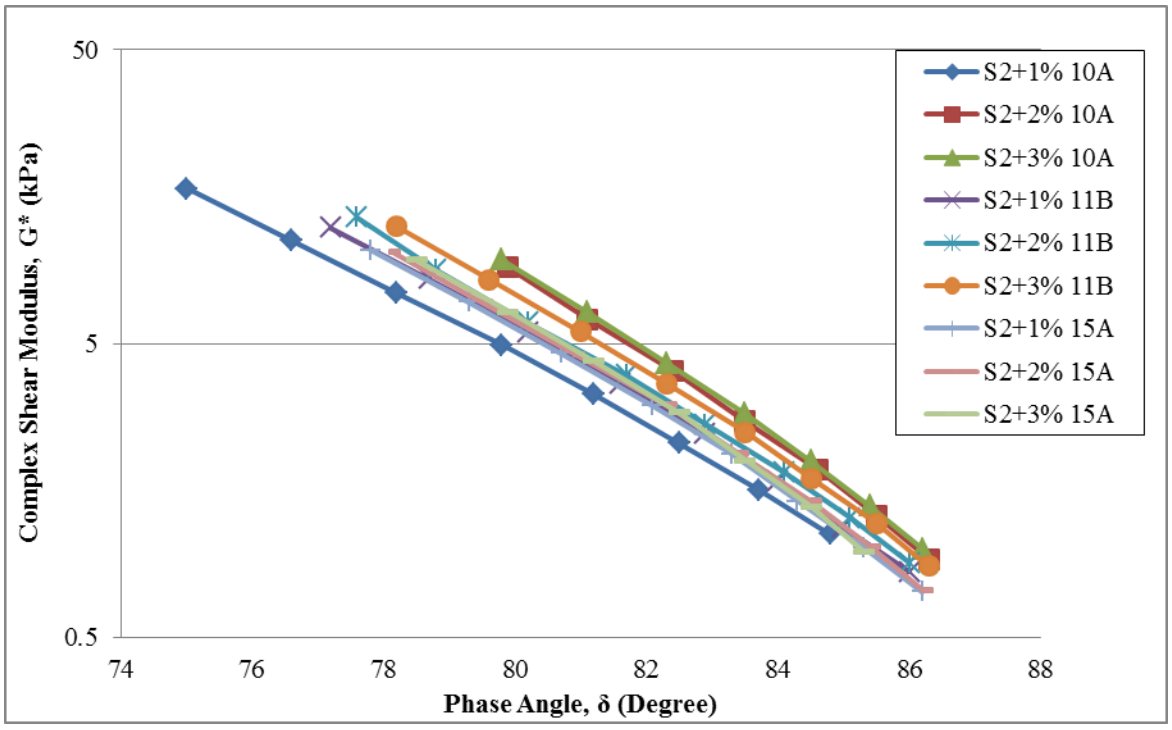

Figure 21. Complex shear modulus (G*) vs. phase angle (δ) curve for Source 2 modified binder.

5.4. Sessile Drop Analysis

An optical Contact Analyzer (OCA) was used to determine the contact angle on the surface of nanoclay-modified asphalt binders. It has been observed that, for binders from both the sources, contact angles were higher in case of water than the ethylene glycol and formamide. However, no comparison could be done between the contact angles for ethylene glycol and formamide.

As discussed before, the surface free energy of any materials can be divided into the following components: acid component, base components, and Lifshitz-van der Waals components. As seen from Figure 262, in most cases for the asphalt binder from Source 1, the acid components for Cloisite 10A and Cloisite 11B modified binders were found to be lower than the unmodified binders. On the other hand, the Liftshitz-van der Waals components were found higher in the Cloisite 10A and Cloisite 11B modified binders than in the Cloisite 15A modified binders. Finally, the total surface free energies were found to be very close for all the modified and unmodified binders from Source 1. On the other hand, the binder with the 3% Cloisite 10A was found to be the binder with the highest work of cohesion, which indicated the highest binder-to-binder bond strength when Source 1 binder was modif ied (Figure 23).

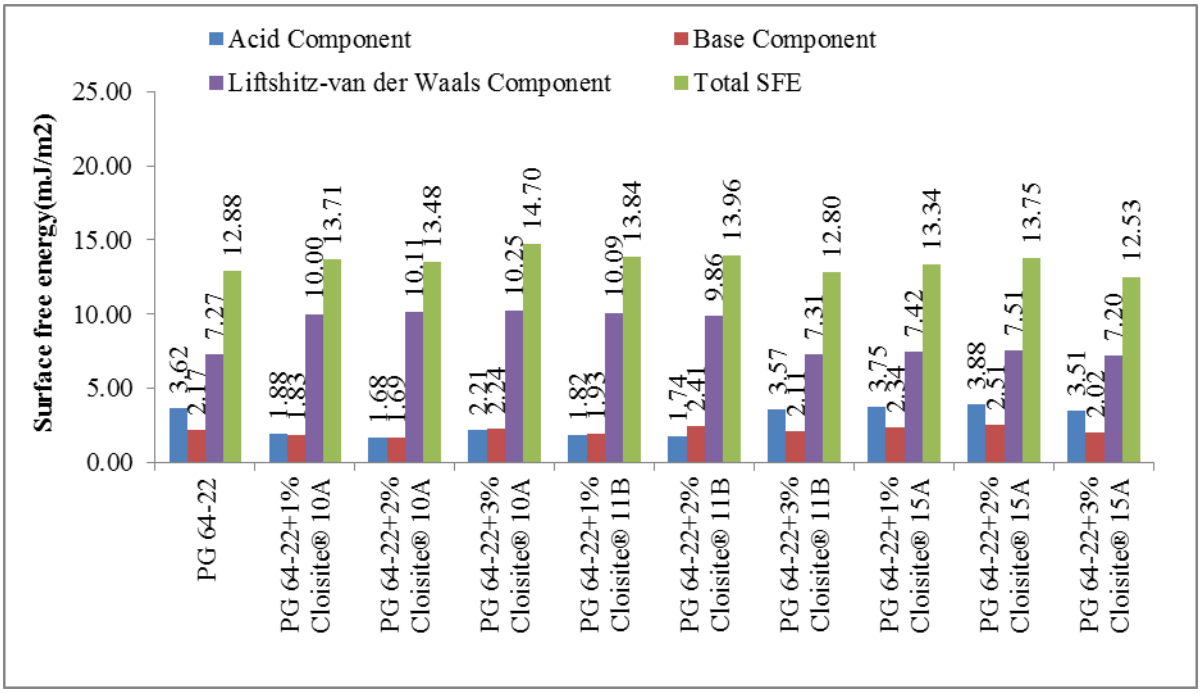

Figure 22. Surface free energy components for Source 1 binders.

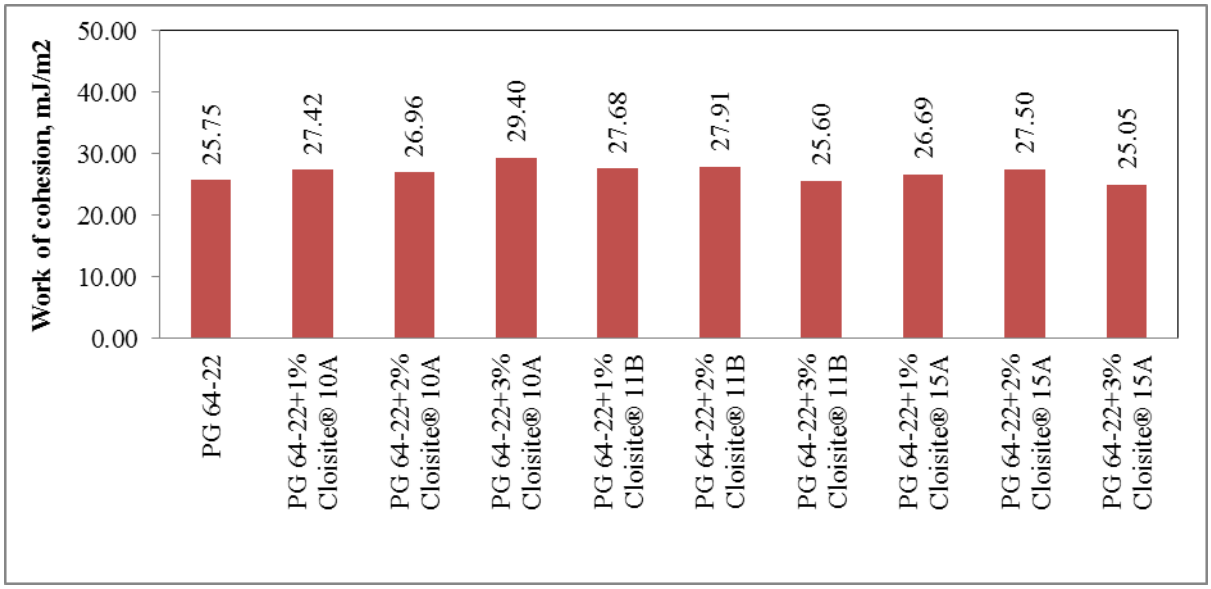

Figure 23. Work of cohesion for the binders of Source 1.

For the binders from Source 2 the acid components, base components, and Lifshitz-van der Waals components were found to be very similar (Figure 24). Therefore, there was no significant change in the total surface energy of the binders from Source 2. For the same reason, the work of cohesion values for the Source 2 binders was very close to each other, indicating that tested nanoclays were not expected to have any adverse effects on binder-to-binder bond strength when Source 2 binder is modified.

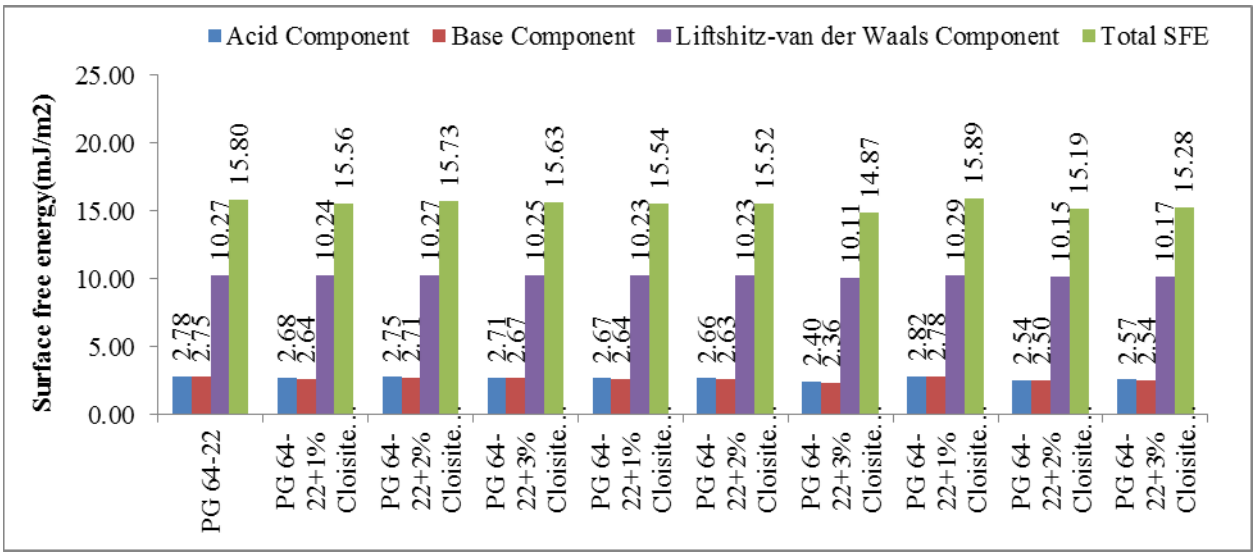

Figure 24. Surface free energy components for Source 2 binders.

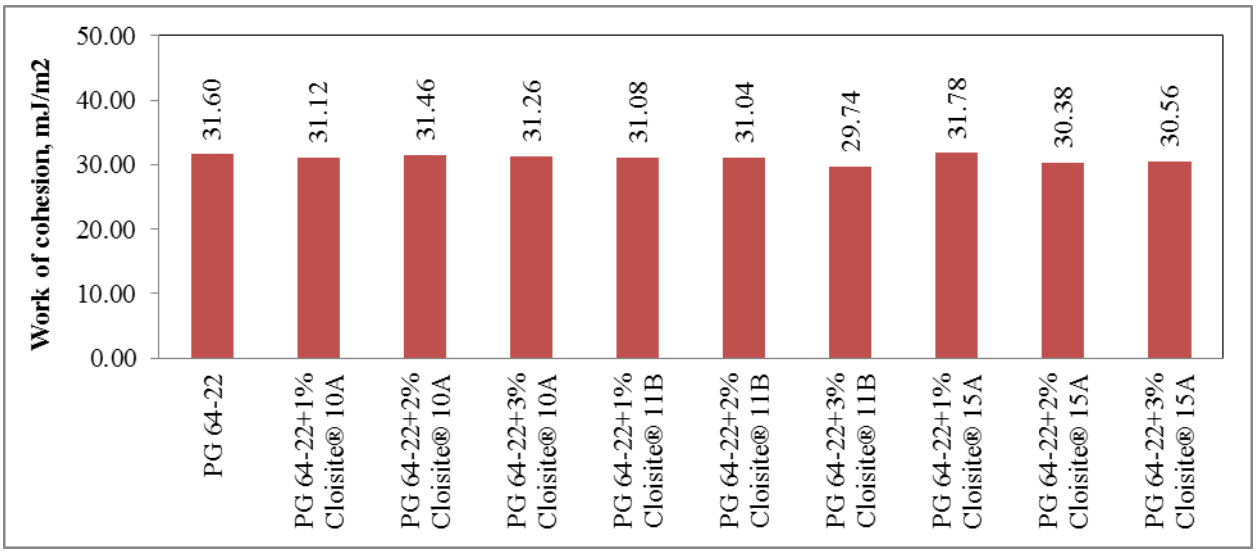

Figure 25. Work of cohesion for the binders of Source 2.

For evaluating stripping resistance of aggregate-binder systems, two types of aggregates (sandstone and limestone gravel) were considered in this study. The aggregate samples were collected from Arkhola, AR. The different components of the surface free energy values of these aggregates are given in Table 4.

Table 4. Different components of SFE for sandstone and gravel *(30)*.

Aggregate Type	Γ ab	Γ LW	Γ (base)	Γ+ (acid)	Γ total
Sandstone	250.3	43.5	555.2	28.2	293.7
Gravel	299.2	57.5	973	23	356.7

From further analysis, in the dry condition, it was found that the adhesive energy values for the Source 1 binders were found to be higher for the Cloisite 15A modified binders. It was also observed that the adhesive energy was higher for gravel (limestone) than the sandstone. It can be noted that limestone is basic in nature and sandstone is neutral in polarity. With acidic asphalt binder, it was expected that the limestone-binder system would have better adhesive bonds compared to the sandstone-binder system.

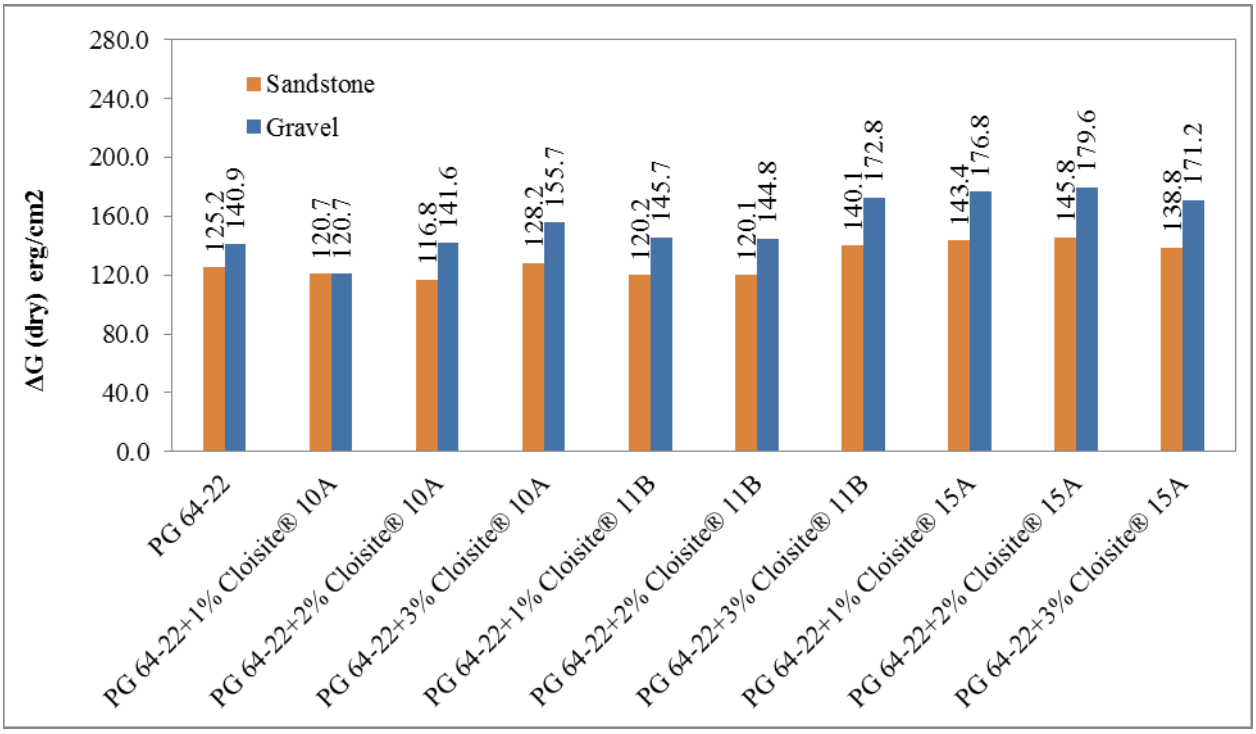

Figure 26. Free energy for the Source 1 binders (dry).

For Source 2 binders (Figure 27), the unmodified binders had higher adhesive energy in the case of sandstone than limestone. But for most cases of the modified Source 2 binders, the adhesive energy in the dry condition was found higher for gravel (limestone) rather than sandstone. The reason for having the more adhesive energy for Source 2 binders compared to Source 1 binders was that Source 2 binders were more acidic in nature, which facilitated higher bond strength with basic limestone.

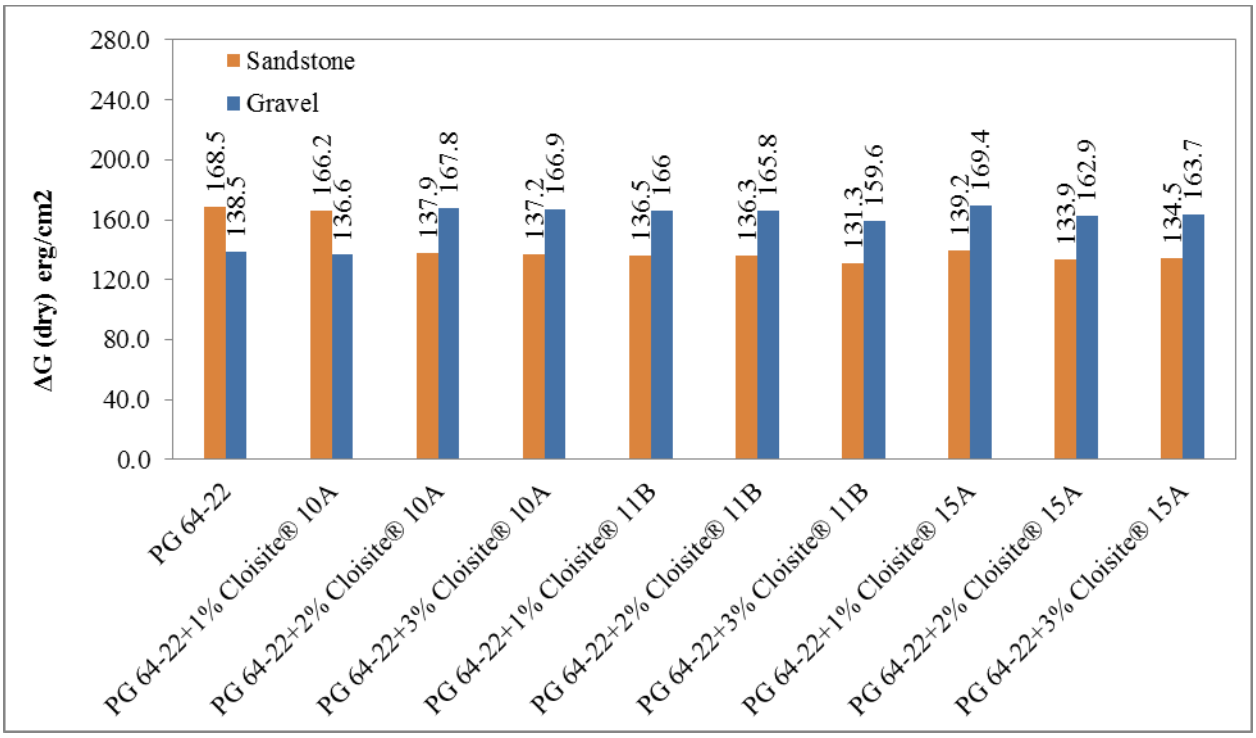

Figure 27. Free energy for the Source 2 binders (dry).

At the wet condition, the debonding energy (negative adhesion energy) becomes higher than the dry condition of the sandstone (Figures 28 and 29). But, the values reduced significantly for the binders with gravel. For the Source 2 binders, the debonding energy was found to be higher only in a few cases. Like the binder with 3% Cloisite modifiers, the debonding energy for sandstone was lower than gravel.

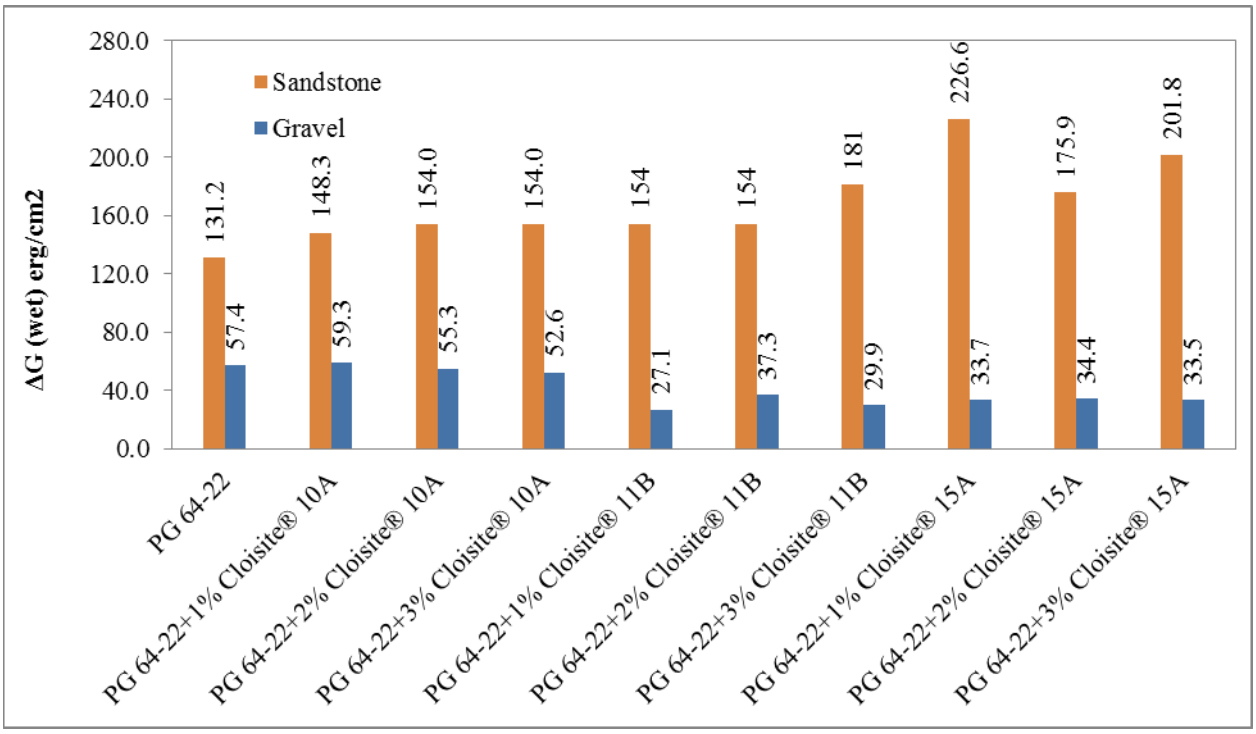

Figure 28. Free energy for the Source 1 binders (wet).

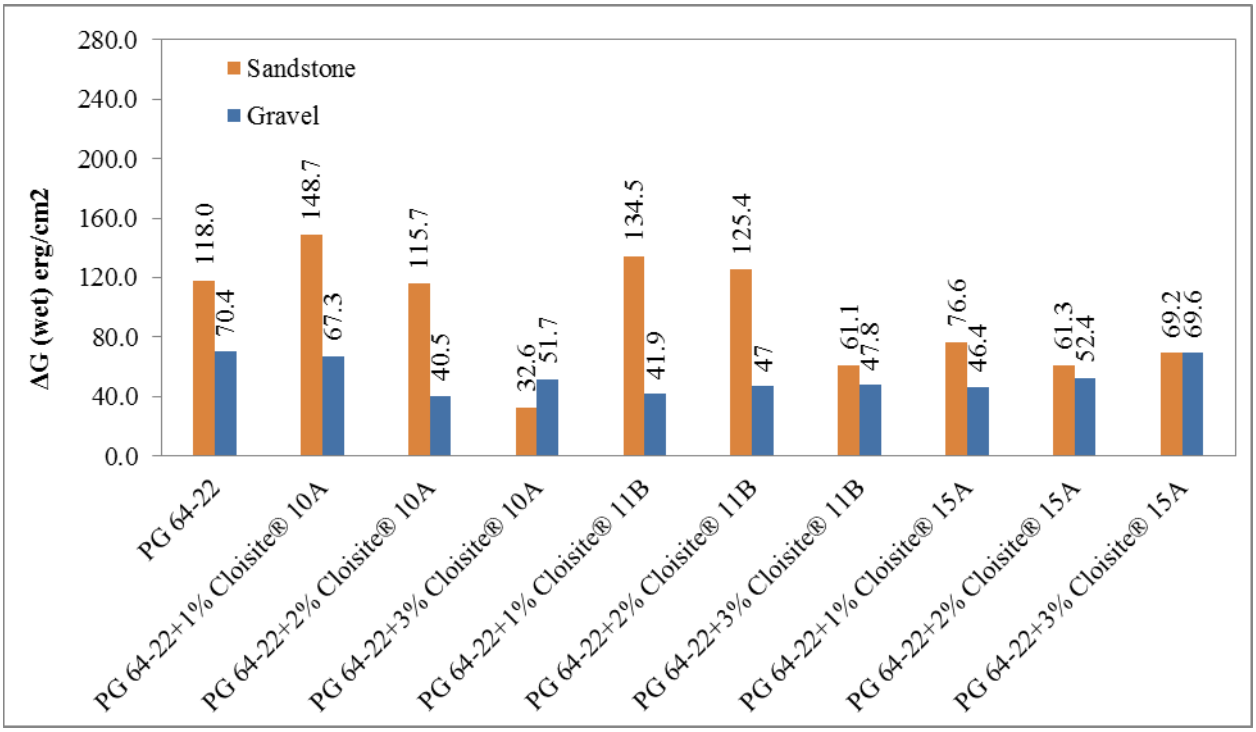

Figure 29. Free energy for the Source 2 binders (wet).

The compatibility ratio for the Source 1 binders remained below 1 with sandstone. But for gravel, the compatibility ratio is higher for the gravel which started from 2 to above 5 (Figure

30). This always signifies good bonding condition between the modified binder and gravel. It is considered that a compatibility ratio, CR > 1.5 is very good (A), CR from 0.75 to 1.5 is good (B), CR from 0.5 to 0.75 is poor (C), and CR < 0.5 is very poor (D).

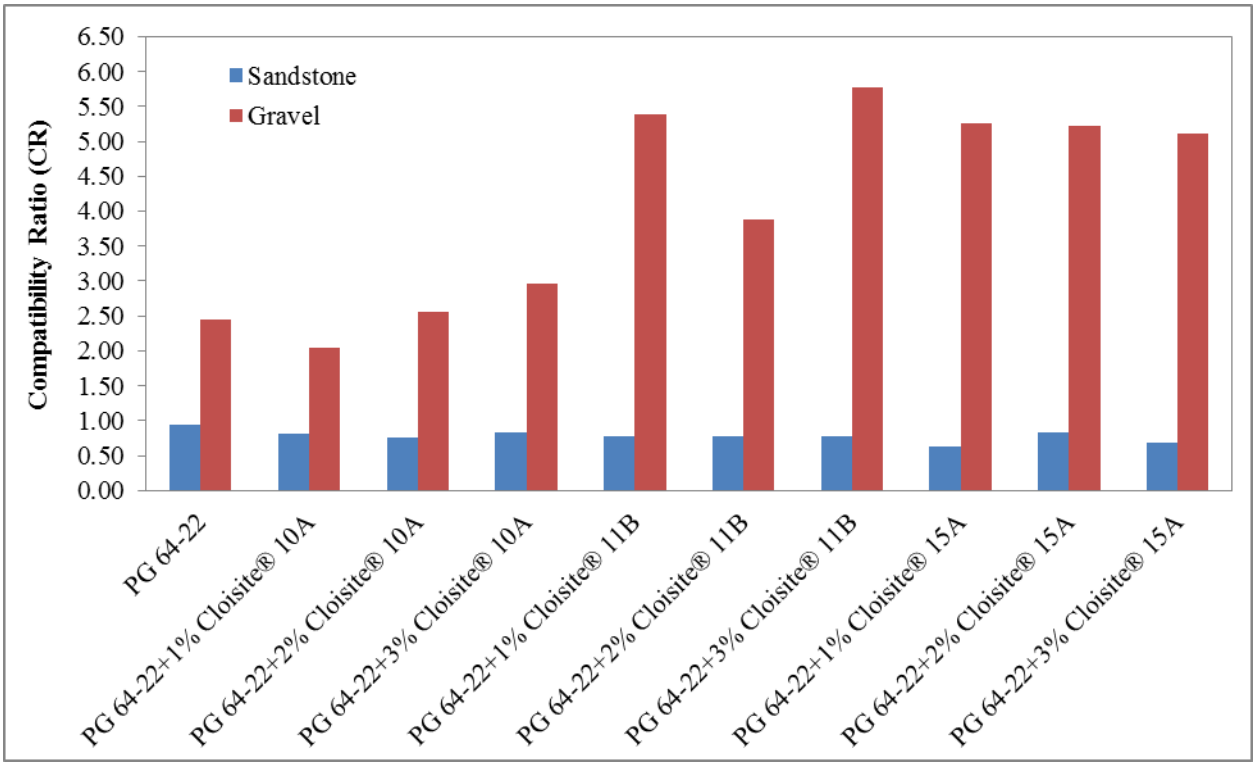

Figure 30. Compatibility ratio for Source 1 binders.

For Source 2 binders, compatibility for the sandstone was found higher than the Source 1 (Figure 31). Moreover, the compatibility ratio for gravel with Source 2 binders remained higher too than sandstone. It could be expected that the nanoclay-modified binders would always provide good bonding with limestone gravel. Tables 4 and 5 represent CR values of all the tested aggregate-binder systems from this study. Please see Appendix E for additional results of the OCA tests.

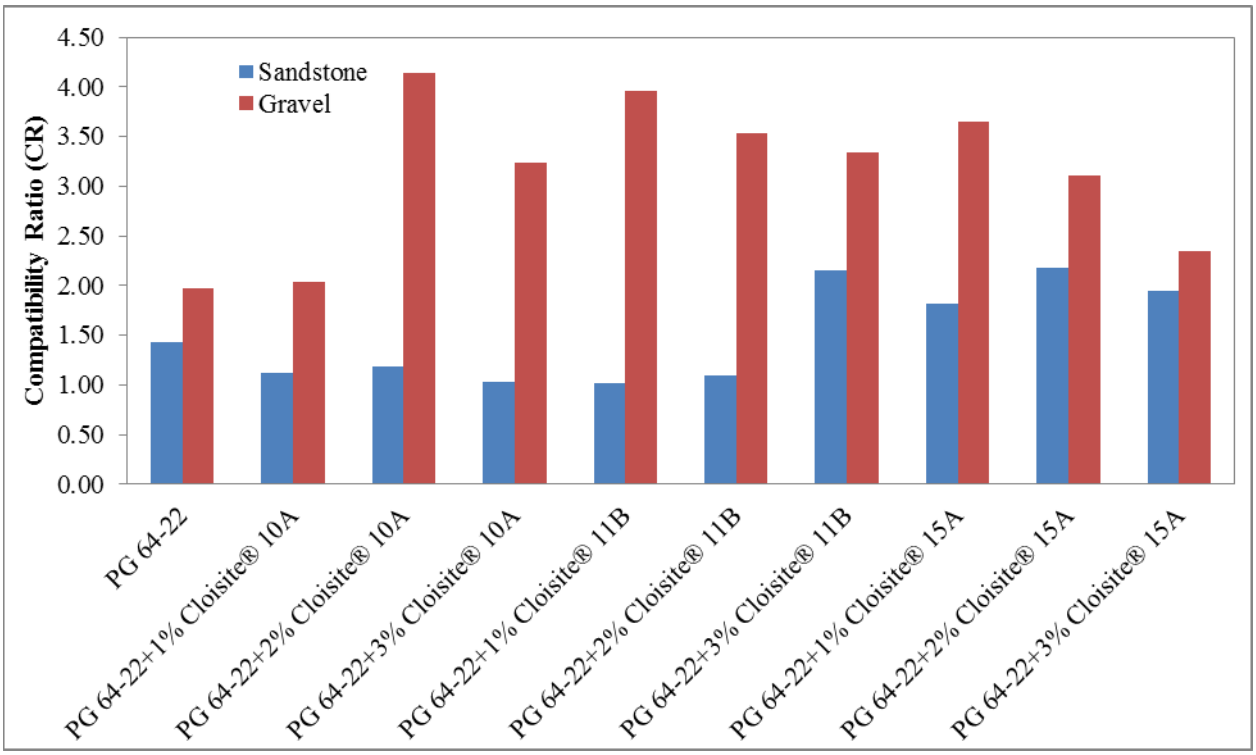

Figure 31. Compatibility ratio for Source 2 binders.

Table 5. Compatibility for Source 1 binders with sandstone and gravel.

Binder type	CR Values for Sandstone	Sandstone	CR Values for Gravel	Gravel
PG 64-22	0.95	B	2.45	A
PG 64-22+1% Cloisite® 10A	0.81	B	2.04	A
PG 64-22+2% Cloisite® 10A	0.76	B	2.56	A
PG 64-22+3% Cloisite® 10A	0.83	B	2.96	A
PG 64-22+1% Cloisite® 11B	0.78	B	5.38	A
PG 64-22+2% Cloisite® 11B	0.78	B	3.88	A
PG 64-22+3% Cloisite® 11B	0.77	B	5.78	A
PG 64-22+1% Cloisite® 15A	0.63	C	5.25	A
PG 64-22+2% Cloisite® 15A	0.83	B	5.22	A
PG 64-22+3% Cloisite® 15A	0.69	C	5.11	A

Table 6. Compatibility for Source 2 binders with sandstone and gravel.

Binder type	CR Values for Sandstone	Sandstone	CR Values for Gravel	Gravel
PG 64-22	1.43	B	1.97	A
PG 64-22+1% Cloisite® 10A	1.12	B	2.03	A
PG 64-22+2% Cloisite® 10A	1.19	B	4.14	A
PG 64-22+3% Cloisite® 10A	1.03	B	3.23	A
PG 64-22+1% Cloisite® 11B	1.01	B	3.96	A
PG 64-22+2% Cloisite® 11B	1.09	B	3.53	A
PG 64-22+3% Cloisite® 11B	2.15	A	3.34	A
PG 64-22+1% Cloisite® 15A	1.82	A	3.65	A
PG 64-22+2% Cloisite® 15A	2.18	A	3.11	A
PG 64-22+3% Cloisite® 15A	1.94	A	2.35	A

5.5. Atomic Force Microscope (AFM)

Morphological and nanomechanical properties such as surface roughness (Figure 32.a), DMT (Derjaguin–Muller–Toporov) modulus (Figure 32.b), adhesion (Figure 32.c), and deformation (Figure 35.d) parameters were measured for unmodified and nanoclay-modified asphalt binders and test data is shown in Table 7. The height sensor value was found to be maximum for the asphalt binder modified by 3% Cloisite 15A and minimum for asphalt binder modified by 1% Cloisite 15A. The DMT modulus was found to decrease for nanoclay-modified asphalt binders. Adhesion and deformation values were also found to decrease for nanoclay-modified asphalt binders. The minimum adhesion and deformation values were found for asphalt binder samples modified with 1% Cloisite 10A.

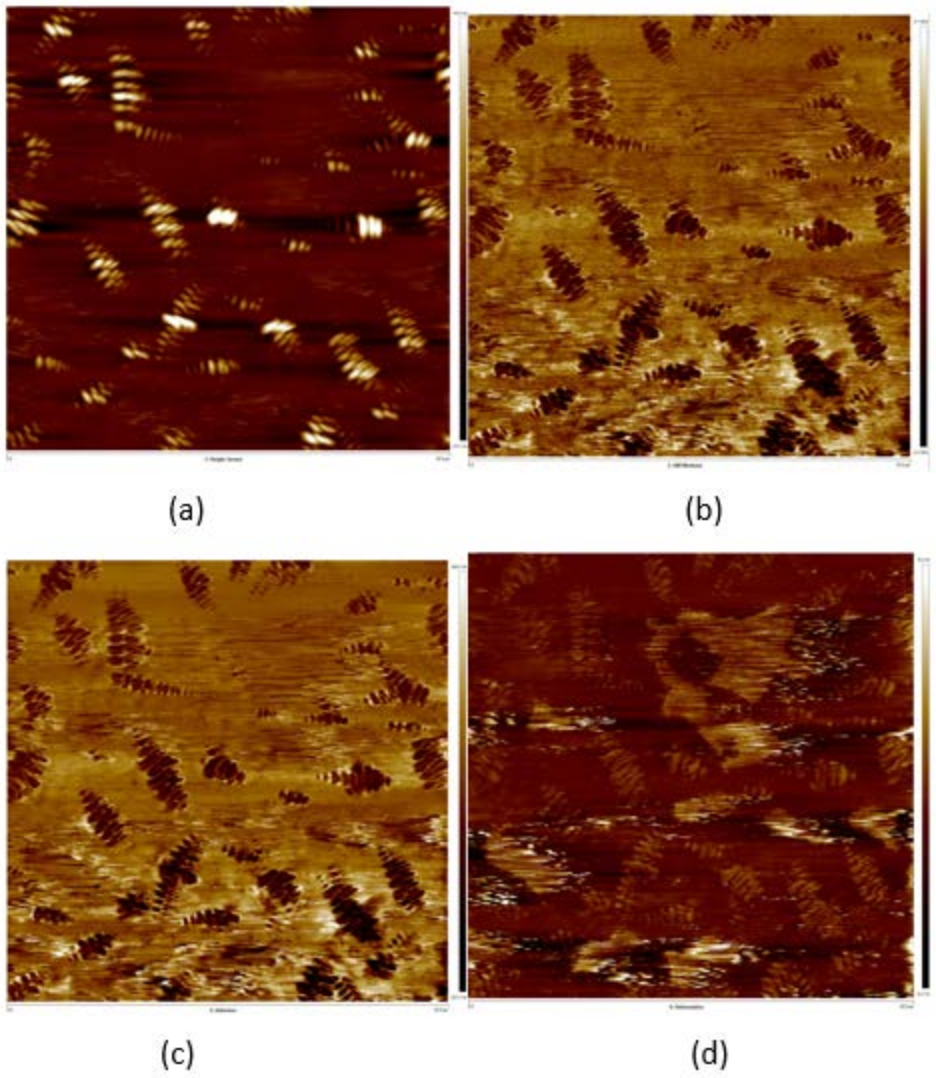

Figure 32. AFM test results (a) Surface roughness, (b) DMT modulus, (c) Adhesion, and (d) Deformation.

Table 7. Value of the morphological and nanomechanical properties.

Sample ID	Average Value of Height Sensor (nm)	Average Value of DMT Modulus (MPa)	Average Value of Adhesion (nN)	Average Value of Deformation (nm)
S1 (Neat Binder)	7.79	3221	362	5.41
S1+1% 10A	7.32	755	73.7	1.94
S1+2% 10A	13.5	1768	222	2.8
S1+3% 10A	6.52	2937	305	5.37
S1+1% 11B	13.7	625	136	4.2
S1+2% 11B	8.36	682	102	3.19
S1+3% 11B	9.32	2081	196	4.41
S1+1% 15A	6.5	694	176	4.21
S1+2% 15A	9.46	1522	163	4.05
S1+3% 15A	15.8	1234	261	3.55

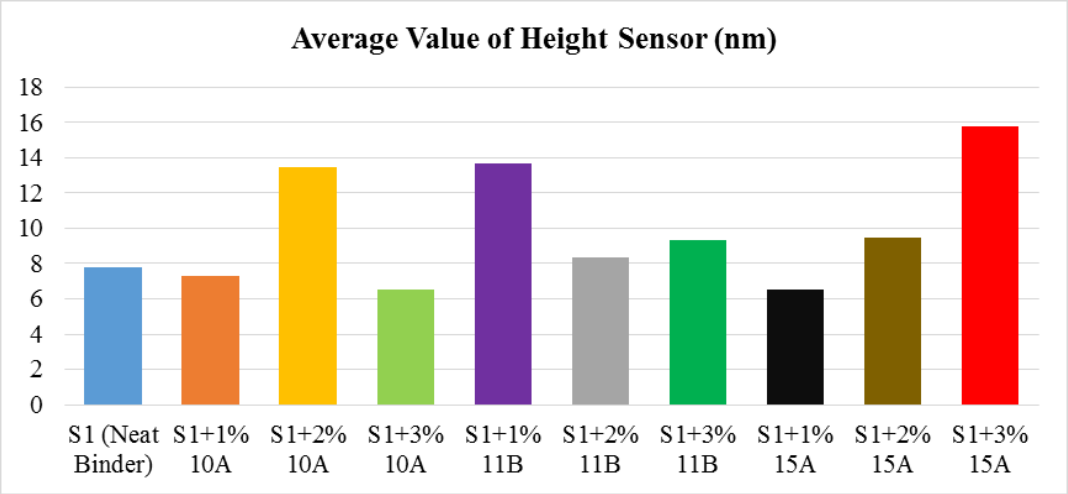

Figure 33. Average value of height sensor for Source 1 modified binders.

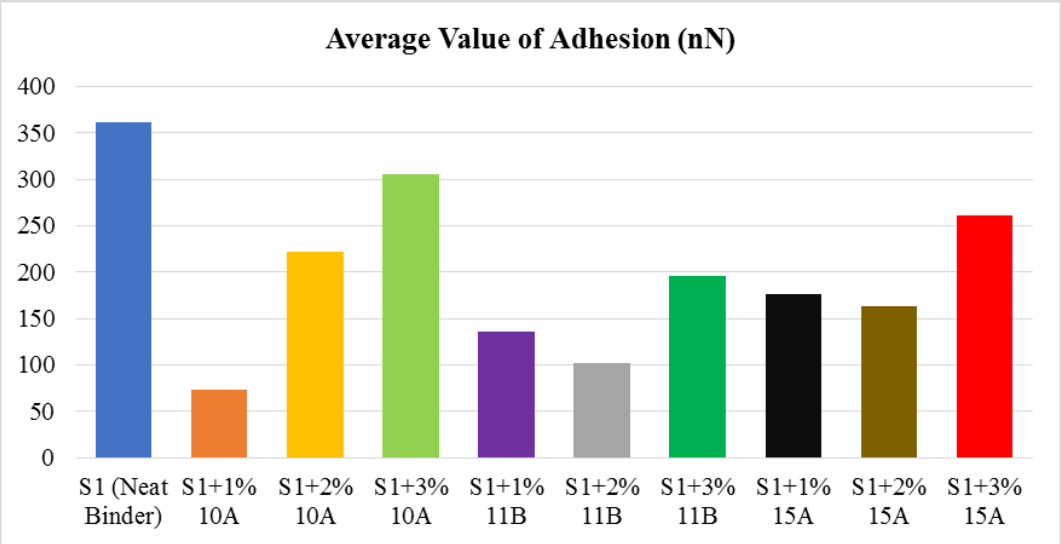

Figure 34. Average value of adhesion for Source 1 modified binder.

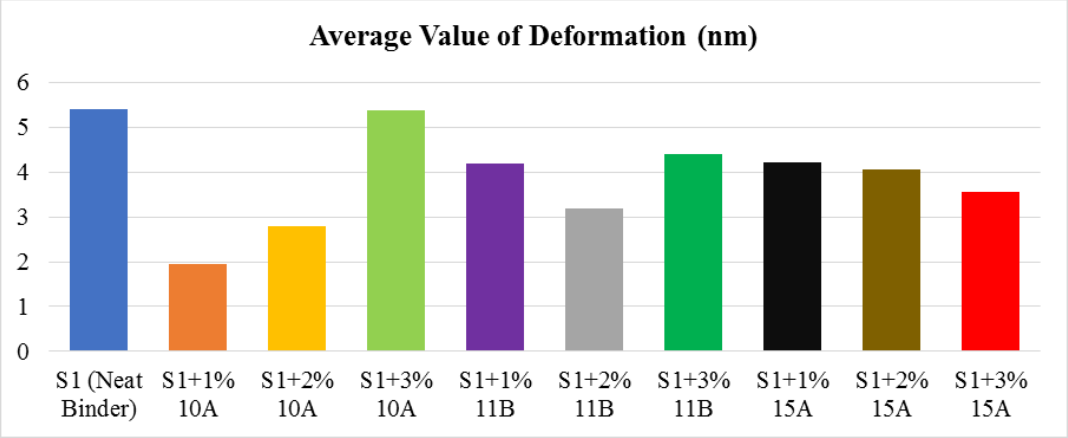

Figure 35. Average value of deformation for Source 1 modified binder.

5.6. SARA Analysis

SARA fractions of the unaged nanoclay-modified asphalt binders were conducted following the specification ASTM D4124-09 *(31)*. The purpose of the chemical analysis was to observe any change due to the chemical modification. The outcomes of the chromatographic separation were reported as the SARA fractions of the nanoclay-modified asphalt binder. The percent SARA fractions for the unaged binders from both sources are reported in Figure 36 and 37.

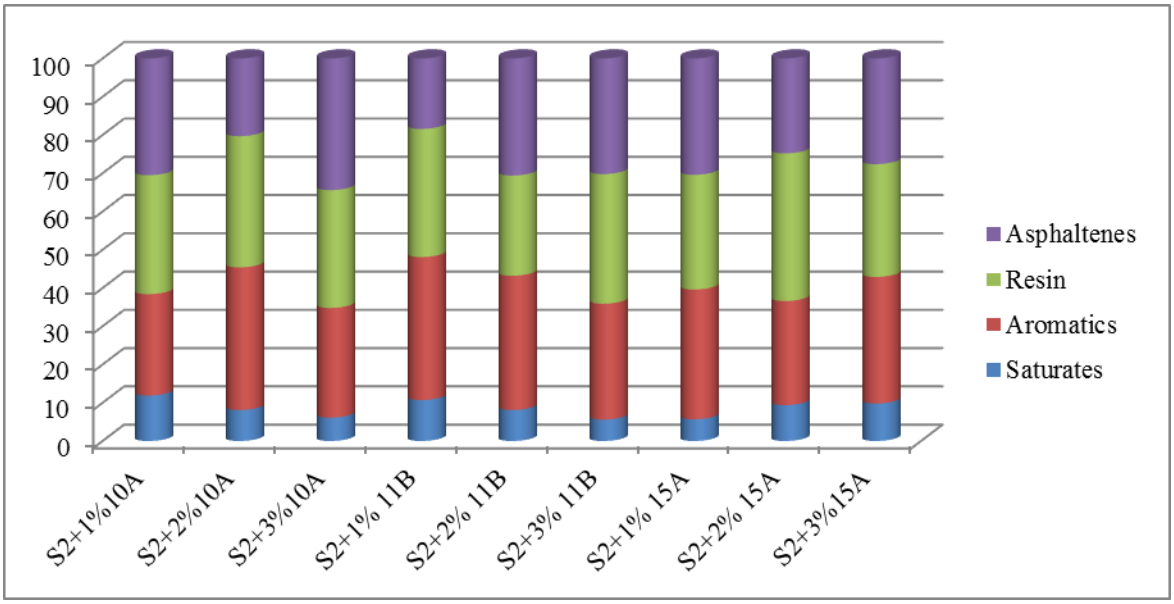

Figure 36. SARA fractions for Source 1 binders.

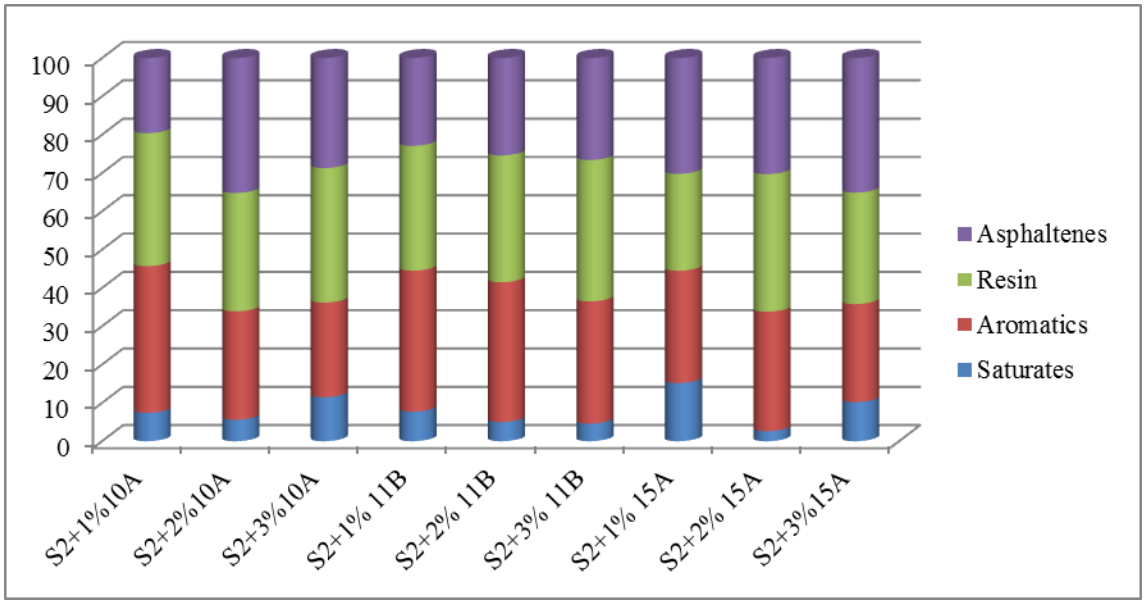

Figure 37. SARA fractions for Source 2 binders.

When an attempt was made to correlate the results of the SARA fractions with the mechanistic properties, it was found that the Asphaltene contents were highly correlated with the rutting

parameter (G*/sinδ), which were obtained from DSR test results. Using the DSR results, an inversely linear relationship was found between the percentage of the Asphaltene content and rutting parameter which means that with the increase of the Asphaltene contents, the rutting parameter would decrease. Among the binders from the Source 1, the sample with 3% 10A nanoclay modification showed the lowest rutting parameter and from Source 2, the binder with 2% 10A nanoclay modification exhibited the lowest rutting parameters. The correlation between these two parameters is shown in Figure 38 and 39. Please see Appendix F for additional results of the SARA analysis.

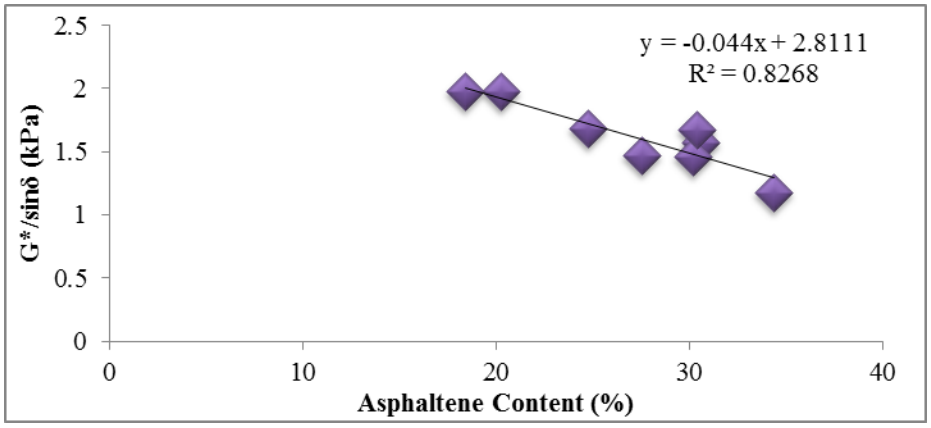

Figure 38. Correlation between asphaltene content and rutting parameters for Source 1 binders.

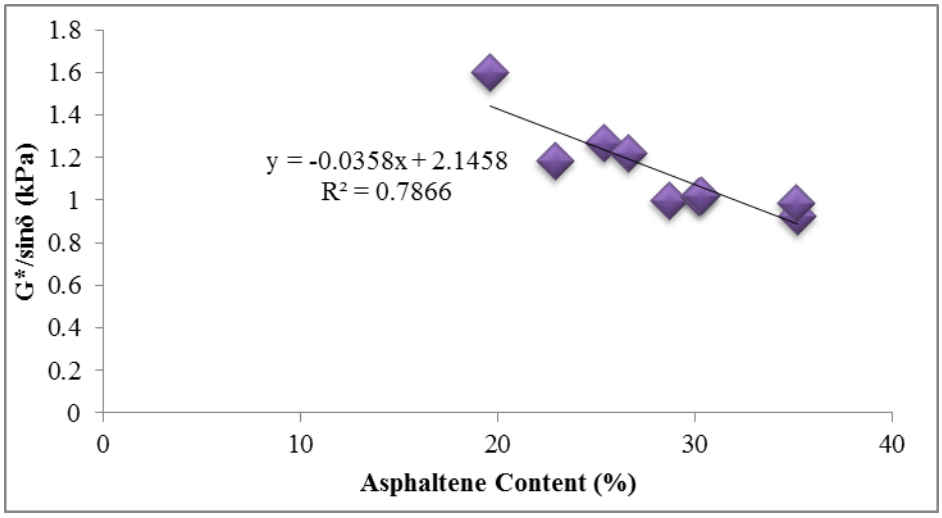

Figure 39. Correlation between asphaltene content and rutting parameters for Source 2 binders.

It was also observed that the Asphaltene contents have a significant impact on the viscosity of the binders also (Figures 40 and 41). With the increase of the Asphaltene contents of the nanoclay-modified asphalt binders, the viscosity at 135°C decreases gradually. From the Source 1 binders, at 135°C, asphalt binder with 2% nanoclay showed higher viscosity than other modified binders. In the case of the binders from Source 2, modification with 1% 10A gives the highest value of viscosity at 135°C. So, it is quite clear that nanoclay 10A performs better as a

modifier than nanoclay 11B and nanoclay 15A while considering rutting parameters and viscosity.

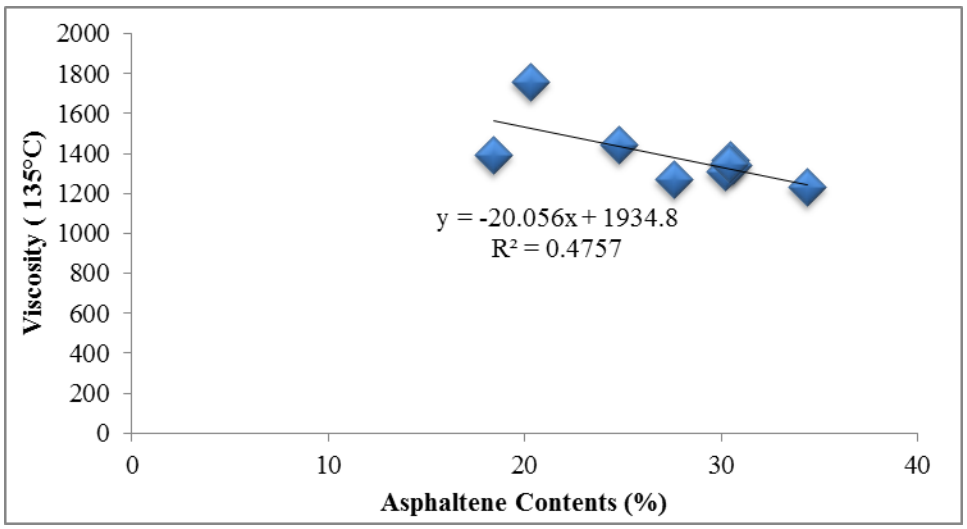

Figure 40. Correlation between asphaltene content and viscosity for Source 1 binders.

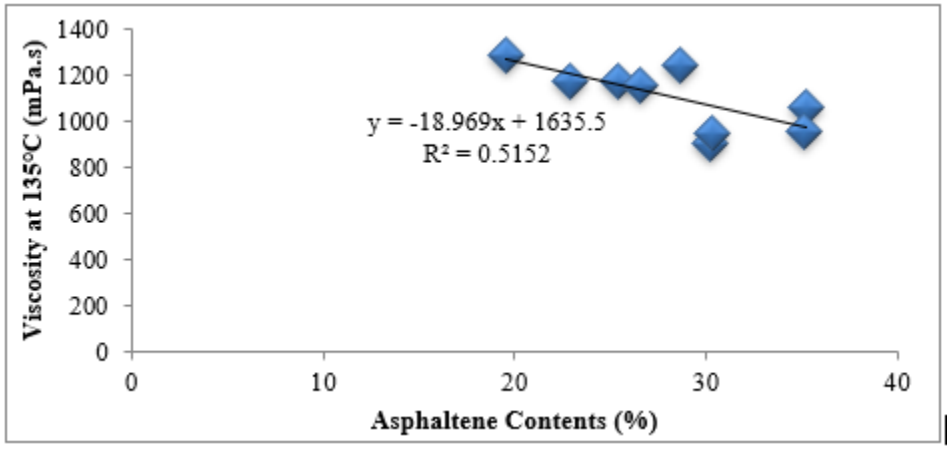

Figure 41. Correlation between asphaltene content and viscosity for Source 2 binders.

5.7. Cost Analysis

5.7.1. Life Cycle Cost Analysis

For the life cycle cost analysis of the project, LCCAExpress 2.0 has been used. A cost analysis was conducted for a road segment of 5 miles. The road was assumed to be a two-lane highway with 4 ft. shoulders on both sides. The operating speed was 55 mph. The analysis was conducted for a period of 40 years with a discount rate of 4%. The current consumer price index (CPI), which is a measure of a weighted average of prices of a basket of consumer goods and services was found to be 173.644. The total net present value (NPV) was estimated to be $5,333,889 /mile. Unit prices of the various layers of the asphalt pavement were taken from the literature review. The unit prices of different layers of the asphalt pavement are given in Table 8.

Table 8. Costs of different unit prices in asphalt pavement.

Sector	Price	Unit
HMA Wearing Course:	36	$/ton
HMA Binder Course:	35	$/ton
HMA Base Course:	35	$/ton
Aggregate Base:	36.24	$/ton
Asphalt Milling:	1.4	$/sy
Asphalt Patching:	90	$/ton
Miscellaneous:	0	$/mile
Mobilization:	5	% of total construction cost
Traffic Control:	5	% of total construction cost

The life cycle cost analysis was done by dividing the life cycle into different stages. The initial stage was the complete construction of the pavement. It was considered that only periodic maintenance would be required to keep the pavement functioning throughout the whole life cycle. The cost associated with various stages of the pavement is given in Tables 8 and 9.

Table 9. Net cost of the asphalt pavement.

Activity	Agency	User Delay
Initial Construction	$2,252,623	$422
1st Overlay	$1,224,577	$314
2nd Overlay	$827,280	$235
3rd Overlay	$558,881	$175
4th Overlay	$469,231	$151
Recurring Maintenance	$-	Not Applicable
Other Activities	$-	Not Applicable
Subtotal	$5,332,592	$1,297
Total NPV, $/mile	$5,333,889	

5.7.2. Material cost comparison

One of the primary purposes of the nanoclay modification of asphalt was to find a cost-effective alternative binder for the pavement construction. Currently, Styrene-Butadiene-Styrene (SBS) polymer is predominately used to enhance the properties of the asphalt binder which increases the overall binder cost. Based on the information from several sources, cost per metric ton of PG 64-22 binder was $532.50 in 2013 *(30)*. For PG 70-28 and PG 76-28, the cost per metric ton is $798 and $1064 respectively. The unit cost per metric ton polymer-modified binder ranges from 50-100% more than the neat asphalt binder which associates the increment of 10-20% more than the nanoclay-modified asphalt. One of the more advantageous facts about nanoclay is, it is naturally abundant. So, it could be expected that nanoclay-modified asphalt binders will be a cheaper alternative to polymer-modified asphalt binders. Comparing the cost of a 5-mile highway strip, it was found that using the nanoclay-modified asphalt binder may reduce the asphalt associate cost up to 35%. The result of the cost analysis is summarized in Table 11.

Table 10. Detail information of cycle cost analysis.

	Initial Construction	1st Overlay	2nd Overlay	3rd Overlay	4th Overlay
Year:	0	10	20	30	35
HMA Wearing Course, in.:	1	1	1	1	2
HMA Wearing Course, pcf:	145	145	145	145	145
HMA Binder Course, in.:	2.5	2.5	2.5	2.5	2.5
HMA Binder Course, pcf:	145	145	145	145	145
HMA Base Course, in.:	6	0	0	0	0
HMA Base Course, pcf:	145	145	145	145	145
Aggregate Base, in.:	6	0	0	0	0
Aggregate Base, pcf:	115	115	115	115	115
Miscellaneous:	0	0	0	0	0
Milling, sy:	88,000	0	0	0	0
Patching, ton:	88,000	88,000	88,000	88,000	88,000
Days to Complete:	5	5	5	5	5

Table 11. Material cost comparison between SBS and nanoclay-modified PG 64-22 binders.

Estimated cost for SBS-modified binders	Estimated cost for nanoclay-modified binders	Material cost reduction
$11,006.24	$39,872.00	35%

6. CONCLUSIONS

Due to the nanoparticle addition and nanoscale dispersion, modified asphalt binders became one of the most promising materials. In this study, nanoclay-modified asphalt binders were tested in the laboratory. A high shear mixer was used for mixing nanoclay with neat binder to make good dispersion. Viscosity was found to increased significantly (up to 187%) due to use of different percentage compared to neat binder. Both unaged and RTFO-aged modified binder were used for the DSR test. The complex shear modulus increased, and the phase angle decreased significantly. Based on the findings of this limited study, rutting resistance was expected to increase significantly due to the addition of nanoclay. Morphological and nanomechanical analysis was conducted from atomic force microscope (AFM) test results. The adhesion and deformation values decreased. But, the surface roughness did not vary significantly. Based on the results, it could be said that Cloisite 10A and Cloisite 11B have high potential to become alternatives of polymers. But, further test results and field performance data are required to establish this idea. In the Sessile Drop test results, the work of cohesion values were found to be higher with respect to base binder. Also, a very good compatibility ratio was also observed for nanoclay modified binders with gravel. From the SARA analysis of the unaged nanoclay-modified asphalt binders, correlations were found between the SARA fractions and the mechanistic properties of the binder. From the regression analysis, it was observed that mechanical properties like viscosity, rutting parameter etc. are correlated with the asphaltene fractions of the modified asphalt binders. The percentage of asphaltene content increased and percentage of saturate content decreased due to the short-term (RTFO) and long-term (PAV) aging of nanoclay-modified asphalt binders. Based on life-cycle cost analysis, it is observed that nanoclay is expected to reduce the materials cost of asphalt up to 35% compared to the SBS-modified binders.

7. RECOMMENDATIONS

The current study has been limited to selected laboratory testing of asphalt binders modified with three different types of nanoclays. Additional testing is required to have a better understanding of the performance of nanoclays-modified binders and mixes. Thus, the following research initiatives can be undertaken:

- Based on the limited laboratory test results and cost analyses, asphalt binder modified with certain nanoclays (2% Cloisite 10A and 1% Cloisite 11B) were found to be viable alternatives of SBS polymer in modifying asphalt binders.
- For laboratory investigations, a high shear mixer is recommended for blending nanoclay with a binder. Blending protocol with rotation 2000 rpm, temperature 150°C and mixing duration 2 hours were suitable for mixing the nanoclay with binders.
- A suitable blending protocol was developed for wet mixing the nanoclay with neat binders using a high shear mixture. Further investigation is needed to transfer the idea of laboratory mixing protocol in the field (refinery or mixing plant). It is still unknown whether dry mixing or wet mixing of nanoclays with neat binders will be the better choice. The dry mixing refers to mix nanoclays in the asphalt mixing plant, whereas the wet mixing is to mix nanoclays with asphalt binders.
- Mixture tests that estimate rutting, fatigue and low temperature cracking resistance reflecting the field condition are necessary for establishing a strong recommendation for nanoclay-modified binders.
- A field demonstration project is highly recommended before putting nanoclay-modified asphalt in practice.

REFERENCES

1. Gierhart, D. (2011). “Use of WMA and RAP in Oklahoma.” Rep. Prepared for the Asphalt Institute, Lexington, KY.

2. ARDOT (2018). Arkansas Department of Transportation Monthly Asphalt Binder Price Index. As per "Price Adjustment for Asphalt Binder" Special Provision, Little Rock, AR.

3. ARDOT (2017). ARDOT Pricing Data. Arkansas Department of Transportation Program, Management Division. Weighted Average Unit Prices for The Year 2017, Little Rock, AR.

4. You, Z., Mills-Beale, J., Foley, J. M., Roy, S., Odegard, G. M., Dai Q., and Goh, S. W. (2011). “Nanoclay-modified Asphalt Materials: Preparation and Characterization.” *Construction and Building Materials* 25, 1072-1078.

5. Liu, G. W. (2010). Characterization of organic surfactant on montmorillonite nanoclay to. In *J. Mater. Civ. Eng., 10.1061* (pp. 794–799).

6. Hossain, Z., Zaman, M., Saha, M. C., and Hawa, T. (2014) “Evaluation of Viscosity and Rutting Properties of Nanoclay-Modified Asphalt Binders.” Geo-Congress 2014 Technical Papers: Geo-Characterization and Modeling for Sustainability. 3695-3702.

7. Yao, H., You, Z., Li, L., Shi, X., Goh, S. W., Mills-Beale, J., and Wingard, D. (2012). “Performance of Asphalt Binder Blended with Non-modified and Polymer-modified Nanoclay.” *Construction and Building Materials 35*, 159-170.

8. Zhang, H., Su. M., Zhao, S., Zhang, Y., and Zhang, Z. (2016). “High and Low Temperature Properties of Nano-particles/Polymer Modified Asphalt.” *Construction and Building Materials*, Vol. 114, 323-332.

9. Abdullah, M. E., Zamhari, K. A., Hainin, M. H., Oluwasola, E. A., Hassan, N. A., and Yusoff, N. I. M. (2016). “Engineering Properties of Asphalt Binders Containing Nanoclay and Chemical Warm-mix Asphalt Additives.” *Construction and Building Materials*, Vol. 112, 232-240.

10. Melo, J. V. S. D., and Triches, G. (2017). “Evaluation of Properties and Fatigue Life Estimation of Asphalt Mixture Modified by Organophilic Nanoclay.” *Construction and Building Materials*, Vol. 140, 364-373.

11. Hauser, E., and Colombo, U. (1953). “Colloid Science of Montmorillonites and Bentonites.” J. Clays Clay Miner., 2(1), 439–461.

12. Ray, S. S., and Okamoto, M. (2003), “Polymer/layered Silicate Nanocomposites: A Review from Preparation to Processing.” *Prog. Polym. Sci*. 28, 1539–1641.

13. Jahromi, S. G., and Khodaii, A. (2009). “Effects of Nanoclay on Rheological Properties of Bitumen Binder.” *Construction and Building Materials* 23, 2894-2904.

14. Ghile, D. B. (2005). “Effects of Nanoclay Modification on Rheology of Bitumen and on Performance of Asphalt Mixtures.” Master’s Thesis, Delft University of Technology, Netherlands.

15. Yu, J., Zeng, X., Wu, S., Wang, L., and Liu, G. (2007). “Preparation and Properties of Montmorillonite Modified Asphalts.” *Materials Science and Engineering A* 447, 233–238.

16. Polacco, G., Filippi, S., Stastna, J., Biondi, D., and Zanzotto, L., (2008) “Rheological Properties of Asphalt/SBS/clay blends.” Eur Polym J;44:35, 12–21.

17. Zapién-Castillo, S., Rivera-Armenta, J. L., Chávez-Cinco, M. Y., Salazar-Cruz, B., A., and Mendoza-Martínez, A. M. (2016). “Physical and Rheological Properties of Asphalt Modified with SEBS/montmorillonite nanocomposite.” *Construction and Building Materials* 106. 349–356.

18. Hossain, Z., Rashid, F., Mahmud, I., and Rahaman, M. (2016). Morphological and Nanomechanical Characterization of Industrial and Agricultural Waste–Modified Asphalt Binders. *Int. J. Geomech.,* 10.1061/(ASCE)GM.1943-5622.0000767 , 04016084.

19. De Moraes, M. B., Pereira, R. B., Simão, R. A., and Leite, L. F. M. (2010). High Temperature AFM study of CAP 30/45 Pen Grade Bitumen. *Journal of Microscopy*, 239(1), 46-53.

20. Dourado, E. R., Simao, R. A., and Leite, L. F. M. (2011). Mechanical Properties of Asphalt Binders Evaluated by Atomic Force Microscopy. *Journal of Microscopy*, 245(2), 119-128.

21. Masson, J. F., Leblond, V., and Margeson, J. (2006). Bitumen Morphologies by Phase-Detection Atomic Force Microscopy. *Journal of Microscopy*, 221(1), 17-29.

22. Jahangir, R., Little, D., and Bhasin, A. (2015). Evolution of Asphalt Binder Microstructure due to Tensile Loading Determined using AFM and Image Analysis Techniques. *International Journal of Pavement Engineering*, 16(4), 337-349.

23. Nahar, S. N., Schmets, A. J. M., Schitter, G., and Scarpas, A. (2014). Quantitative nanomechanical property mapping of bitumen micro-phases by peak-force atomic force microscopy. Proc., 12th ISAP Conference on Asphalt Pavements. North Carolina, USA.

24. Fischer, H., Stadler, H., and Erina, N. (2013). Quantitative Temperature-depending Mapping of Mechanical Properties of Bitumen at the Nanoscale using the AFM Operated with PeakForce TappingTM Mode. *Journal of Microscopy*, 250(3), 210-217.

25. Yu, X., Burnham, N. A., Mallick, R. B., and Tao, M. (2013). A Systematic AFM-based Method to Measure Adhesion Differences between Micron-sized Domains in Asphalt Binders. Fuel, 113, 443-447.

26. Allen, R., Little, D., Bhasin, A., and Lytton, R. (2013). Identification of the Composite Relaxation Modulus of Asphalt Binder using AFM Nanoindentation. *J. Mater. Civ. Eng.*, 10.1061/(ASCE)MT.1943-5533.0000615, 530-539.

27. Tarefder, R. and Zaman, A. (2010). Nanoscale Evaluation of Moisture Damage in Polymer Modified Asphalts. Journal of Materials in Civil Engineering, 10.1061/(ASCE)MT.1943-5533.0000072, 714-725.

28. Cheng, D. X., Little, D. N., Lytton, R. L., and Holste, J. C. (2002). “Surface Free Energy Measurement of Asphalt and its Application to Predicting Fatigue and Healing in Asphalt Mixtures.” Transportation Research Record 1810, Transportation Research Board, Washington, DC, 44–53.

29. Bhasin, A., Button, J. W., and Chowdhury, A. (2005). “Evaluation of Selected Laboratory Procedures and Development of Databases for HMA.” Rep. No. Federal Highway Administration (FHWA)/Texas (TX)-05/0-4203-3, Texas Transportation Institute, Texas A&M Univ., College Station, TX.

30. Hossain, Z., Zaman, M., Hawa, T. and Saha, M.C. (2015).“Evaluation of Moisture Susceptibility of Nanoclay-Modified Asphalt Binders through the Surface Science Approach.” *Journal of Materials in Civil Engineering*, ASCE, 27(10): 04014261.

31. STM D4124-09(2018), Standard Test Method for Separation of Asphalt into Four Fractions, ASTM International, West Conshohocken, PA, 2018, www.astm.org.

APPENDIX A. NAMING CONVENTION

Table A.1. Nomenclature for nanoclay modified binders.

Sample Name	Source Binder	Nanoclay
S1	PG 64-22 From Source 1*	Without Modification
S1+1% 10A	Source 1	Modified by 1% Nanoclay Cloisite 10A
S1+2% 10A	Source 1	Modified by 2% Nanoclay Cloisite 10A
S1+3% 10A	Source 1	Modified by 3% Nanoclay Cloisite 10A
S1+1% 11B	Source 1	Modified by 1% Nanoclay Cloisite 11B
S1+2% 11B	Source 1	Modified by 2% Nanoclay Cloisite 11B
S1+3% 11B	Source 1	Modified by 3% Nanoclay Cloisite 11B
S1+1% 15A	Source 1	Modified by 1% Nanoclay Cloisite 15A
S1+2% 15A	Source 1	Modified by 2% Nanoclay Cloisite 15A
S1+3% 15A	Source 1	Modified by 3% Nanoclay Cloisite 15A
S2	PG 64-22 From Source 2**	Without Modification
S2+1% 10A	Source 2	Modified by 1% Nanoclay Cloisite 10A
S2+2% 10A	Source 2	Modified by 2% Nanoclay Cloisite 10A
S2+3% 10A	Source 2	Modified by 3% Nanoclay Cloisite 10A
S2+1% 11B	Source 2	Modified by 1% Nanoclay Cloisite 11B
S2+2% 11B	Source 2	Modified by 2% Nanoclay Cloisite 11B
S2+3% 11B	Source 2	Modified by 3% Nanoclay Cloisite 11B
S2+1% 15A	Source 2	Modified by 1% Nanoclay Cloisite 15A
S2+2% 15A	Source 2	Modified by 2% Nanoclay Cloisite 15A
S2+3% 15A	Source 2	Modified by 3% Nanoclay Cloisite 15A

*Source 1 Binder collected from Ergon at Memphis

**Source 2 Binder collected from Marathon at Catlessburg

Table A.2. Naming convention for blending samples.

Sample ID	Rotation (rpm), Temperature (°C), Mixing Time (h)
Neat Binder	Neat Binder (Source 1)
1500-150-2	1500 rpm, 150 °C, 2 h
1500-150-3	1500 rpm, 150 °C, 3 h
1500-160-2	1500 rpm, 160 °C, 2 h
1500-160-3	1500 rpm, 160 °C, 3 h
2000-150-2	2000 rpm, 150 °C, 2 h
2000-150-3	2000 rpm, 150 °C, 3 h
2000-160-2	2000 rpm, 160 °C, 2 h
2000-160-3	2000 rpm, 160 °C, 3 h

APPENDIX B. ROTATIONAL VISCOSITY (RV) TESTS

Table B.1. Rotational viscosity (RV) tests.

Sample	Temperature (°C)	Reading 1	Reading 2	Reading 3	Average	Standard Deviation
S1	135	500	512.5	500	504.167	7.217
S1	150	250	262.5	250	254.167	7.217
S1	165	150	137.5	150	145.833	7.217
S1	180	75	75	75	75	0.000
S1+1% 10A	135	1375	1363	1363	1367.000	6.928
S1+1% 10A	150	562.5	550	550	554.167	7.217
S1+1% 10A	165	287.5	287.5	300	291.667	7.217
S1+1% 10A	180	175	175	175	175	0.000
S1+1% 10A	195	25	25	25	25	0
S1+2% 10A	135	1750	1763	1763	1758.667	7.506
S1+2% 10A	150	800	800	812.5	804.167	7.217
S1+2% 10A	165	362.5	375	350	362.500	12.500
S1+2% 10A	180	200	200	187.5	195.8333	7.217
S1+2% 10A	195	25	25	25	25	0
S1+3% 10A	135	1225	1237	1237	1233.000	6.928
S1+3% 10A	150	550	550	562	554	6.928
S1+3% 10A	165	250	262.5	262.5	258.3333	7.217
S1+3% 10A	180	150	150	150	150	0
S1+1% 11B	135	1400	1388	1388	1392.000	6.928
S1+1% 11B	150	578.5	575	575	576.167	2.021
S1+1% 11B	165	275	287.5	275	279.167	7.217
S1+1% 11B	180	137.5	137.5	150	141.6667	7.217
S1+2% 11B	135	1350	1337	1337	1341.333	7.506
S1+2% 11B	150	600	600	587.5	595.833	7.217
S1+2% 11B	165	300	300	287.5	295.833	7.217
S1+2% 11B	180	162.5	150	162.5	158.3333	7.217
S1+2% 11B	135	1300	1313	1300	1304.333	7.506
S1+2% 11B	150	600	587.5	587.5	591.667	7.217
S1+2% 11B	165	312.5	312.5	300	308.333	7.217
S1+2% 11B	180	175	175	162.5	170.8333	7.217
S1+1% 15A	135	1350	1350	1337	1345.667	7.506
S1+1% 15A	150	550	562.5	550	554.167	7.217
S1+1% 15A	165	287.5	275	287.5	283.333	7.217
S1+1% 15A	180	137.5	137.5	150	141.6667	7.217
S1+2% 15A	135	1438	1438	1450	1442.000	6.928
S1+2% 15A	150	612.5	625	625	620.833	7.217

Sample	Temperature (°C)	Reading 1	Reading 2	Reading 3	Average	Standard Deviation
S1+2% 15A	165	312	312.5	312.5	312.333	0.289
S1+2% 15A	180	162.5	162.5	150	158.3333	7.217
S1+3% 15A	135	1275	1275	1263	1271.000	6.928
S1+3% 15A	150	562.5	550	550	554.167	7.217
S1+3% 15A	165	287.5	287.5	300	291.667	7.217
S1+3% 15A	180	162.5	162.5	150	158.3333	7.217
S2	135	437.5	450	450	445.833	7.217
S2	150	200	212.5	212.5	208.333	7.217
S2	165	112.5	112.5	112.5	112.500	0.000
S2	180	62.5	62.5	62.5	62.5	0.000
S2+1% 10A	135	1288	1288	1275	1283.667	7.506
S2+1% 10A	150	550	537.5	537.5	541.667	7.217
S2+1% 10A	165	300	287.5	300	295.833	7.217
S2+1% 10A	180	150	150	162.5	154.1667	7.217
S2+2% 10A	135	1050	1063	1075	1062.667	12.503
S2+2% 10A	150	562.5	575	575	570.833	7.217
S2+2% 10A	165	312.5	312.5	300	308.333	7.217
S2+2% 10A	180	150	150	150	150	0.000
S2+2% 10A	195	75	75	75	75.000	0.000
S2+3% 10A	135	1237	1250	1250	1245.667	7.506
S2+3% 10A	150	600	612.5	600	604.167	7.217
S2+3% 10A	165	325	325	337.5	329.167	7.217
S2+3% 10A	180	175	162.5	162.5	166.6667	7.217
S2+1% 11B	135	1150	1188	1175	1171.000	19.313
S2+1% 11B	150	475	487.5	475	479.167	7.217
S2+1% 11B	165	262.5	262.5	250	258.333	7.217
S2+1% 11B	180	125	125	125	125	0.000
S2+2% 11B	135	1175	1175	1163	1171.000	6.928
S2+2% 11B	150	487.5	500	487.5	491.667	7.217
S2+2% 11B	165	250	250	250	250.000	0.000
S2+2% 11B	180	137.5	137.5	137.5	137.5	0.000
S2+3% 11B	135	1150	1163	1163	1158.667	7.506
S2+3% 11B	150	512.5	512.5	525	516.667	7.217
S2+3% 11B	165	262.5	275	262.5	266.667	7.217
S2+3% 11B	180	162.5	162.5	162.5	162.5	0.000
S2+1% 15A	135	912.5	900	900	904.167	7.217
S2+1% 15A	150	400	387.5	400	395.833	7.217
S2+1% 15A	165	212.5	212.5	212.5	212.500	0.000
S2+1% 15A	180	100	112.5	112.5	108.3333	7.217

Sample	Temperature (°C)	Reading 1	Reading 2	Reading 3	Average	Standard Deviation
S2+2% 15A	135	950	950	937.5	945.833	7.217
S2+2% 15A	150	425	425	412.5	420.833	7.217
S2+2% 15A	165	200	212.5	212.5	208.333	7.217
S2+2% 15A	180	100	112.5	112.5	108.3333	7.217
S2+3% 15A	135	950	962.5	962.5	958.333	7.217
S2+3% 15A	150	412.5	425	400	412.500	12.500
S2+3% 15A	165	212.5	225	212.5	216.667	7.217
S2+3% 15A	180	125	125	125	125	0.000

Table B.2. Compaction and mixing temperature.

Sample	Compaction Temperature Low	Compaction Temperature High	Mixing Temperature Low	Mixing Temperature High
S1	Low	High	Low	High
S1	145	150	158	165
S1+1% 10A	162	166	170	174
S1+2% 10A	165	169	172	176
S1+3% 10A	160	164	170	175
S1+1% 11B	162	167	173	179
S1+2% 11B	164	169	175	180
S1+3% 11B	165	170	177	180
S1+1% 15A	163	168	174	179
S1+2% 15A	165	170	176	180
S1+3% 15A	163	168	175	180

APPENDIX C. DYNAMIC SHEAR RHEOMETER (DSR) TEST RESULTS

Table C.1. Dynamic shear rheometer (DSR) test results: unaged binders.

Sample Name	Temp. (C)	G* (kPa)	Avg.	Phase Angle, δ	Avg.	G*/sinδ (kPa)	Avg.	St Deviation
S1	64	1.55	1.58	85.8	85.7	1.560	1.590	0.0436
		1.64		85.7		1.640		
		1.57		85.8		1.570		
	67	1.07	1.10	86.5	86.4	1.080	1.110	0.0361
		1.15		86.4		1.150		
		1.1		86.5		1.100		
	70	0.752	0.77	87.2	87.1	0.753	0.778	0.0293
		0.809		87		0.810		
		0.769		87.2		0.770		
S1+1%10A	76	2.15	2.14	81.5	81.4	2.174	2.171	0.0055
		2.15		81.5		2.174		
		2.14		81.4		2.164		
	79	1.51	1.51	82.6	82.5	1.523	1.523	0.0103
		1.5		82.6		1.513		
		1.52		82.5		1.533		
	82	1.07	1.07	83.7	83.7	1.077	1.077	0.0000
		1.07		83.7		1.077		
		1.07		83.7		1.077		
S1+2%10A	76	2.75	2.74	80.4	80.4	2.789	2.785	0.0063
		2.74		80.5		2.778		
		2.75		80.4		2.789		
	79	1.95	1.95	81.6	81.6	1.971	1.971	0.0000
		1.95		81.6		1.971		
		1.95		81.6		1.971		
	82	1.38	1.38	82.8	82.8	1.391	1.398	0.0058
		1.39		82.8		1.401		
		1.39		82.8		1.401		
S1+3%10A	76	1.63	1.64	83	83.1	1.642	1.652	0.0096
		1.64		83.2		1.652		
		1.65		83.3		1.661		
	79	1.17	1.17	84.2	84.2	1.176	1.176	0.0000
		1.17		84.2		1.176		
		1.17		84.2		1.176		

Sample Name	Temp. (C)	G* (kPa)	Avg.	Phase Angle, δ	Avg.	G*/sinδ (kPa)	Avg.	St Deviation
	82	0.86	0.86	85	8	0.863	0.863	0.0000
		0.86		85		0.863		
		0.86		85		0.863		
S1+1%11B	76	2.8	2.79	79.3	79.3	2.850	2.846	0.0170
		2.78		79.5		2.827		
S1+1%11B	76	2.81	2.79	79.2	79.3	2.861	2.846	0.0170
	79	1.95	1.94	80.6	80.7	1.977	1.969	0.0223
		1.92		81		1.944		
		1.96		80.6		1.987		
	82	1.38	1.37	81.8	81.7	1.394	1.391	0.0259
		1.4		81.6		1.415		
		1.35		81.9		1.364		
S1+2% 11B	76	2.22	2.21	81.5	81.5	2.245	2.238	0.0214
		2.19		81.6		2.214		
		2.23		81.5		2.255		
	79	1.56	1.55	82.7	82.7	1.573	1.566	0.0118
		1.54		82.8		1.552		
		1.56		82.7		1.573		
	82	1.1	1.09	83.9	83.8	1.106	1.103	0.0057
		1.09		83.8		1.096		
		1.1		83.9		1.106		
S1+3% 11B	73	2.93	2.93	81.2	81.1	2.965	2.972	0.0215
		2.96		81.1		2.996		
		2.92		81.2		2.955		
	76	2.04	2.04	82.4	82.4	2.058	2.061	0.0159
		2.06		82.3		2.079		
		2.03		82.5		2.048		
	79	1.45	1.45	83.5	83.5	1.459	1.459	0.0101
		1.46		83.5		1.469		
		1.44		83.5		1.449		
	82	1.03	1.03	84.5	84.5	1.035	1.038	0.0153
		1.05		84.5		1.055		
		1.02		84.5		1.025		
S1+1% 15A	76	2.36	2.35	79.8	79.8	2.398	2.391	0.0219
		2.37		79.7		2.409		
		2.33		79.9		2.367		
	79	1.65	1.64	81.1	81.1	1.670	1.667	0.0259
		1.67		81		1.691		

Sample Name	Temp. (C)	G* (kPa)	Avg.	Phase Angle, δ	Avg.	G*/sinδ (kPa)	Avg.	St Deviation
		1.62		81.2		1.639		
	82	1.17	1.16	82.1	82.1	1.181	1.178	0.0156
		1.18		82.1		1.191		
		1.15		82.2		1.161		
S1+2% 15A	76	2.37	2.36	79.5	79.4	2.410	2.400	0.0098
S1+2% 15A	76	2.35	2.36	79.4	79.4	2.391	2.400	0.0098
		2.36		79.5		2.400		
	79	1.66	1.65	80.7	80.7	1.682	1.675	0.0059
		1.65		80.7		1.672		
		1.65		80.7		1.672		
	82	1.17	1.16	81.7	81.7	1.182	1.179	0.0058
		1.16		81.7		1.172		
		1.17		81.7		1.182		
S1+3% 15A	73	2.97	2.96	79.8	79.8	3.018	3.014	0.0064
		2.97		79.8		3.018		
		2.96		79.9		3.007		
	76	2.07	2.06	81.1	81.1	2.095	2.088	0.0120
		2.07		81.1		2.095		
		2.05		81.2		2.074		
	79	1.46	1.45	82.2	82.2	1.474	1.463	0.0179
		1.46		82.2		1.474		
		1.43		82.4		1.443		
	82	1.04	1.03	83.2	83.2	1.047	1.037	0.0177
		1.04		83.2		1.047		
		1.01		83.4		1.017		
S2	61	2.44	2.38	86.1	86.2	2.446	2.392	0.0685
		2.41		86.2		2.415		
		2.31		86.3		2.315		
	64	1.66	1.62	86.8	86.8	1.663	1.622	0.0460
		1.63		86.9		1.632		
		1.57		86.9		1.572		
	67	1.14	1.11	87.4	87.4	1.141	1.114	0.0379
		1.13		87.5		1.131		
		1.07		87.5		1.071		
S2+1% 10A	76	2.29	2.28	82.5	82.5	2.310	2.303	0.0058
		2.28		82.5		2.300		
		2.28		82.5		2.300		
	79	1.59	1.59	83.7	83.7	1.600	1.600	0.0000

Sample Name	Temp. (C)	G* (kPa)	Avg.	Phase Angle, δ	Avg.	G*/sinδ (kPa)	Avg.	St Deviation
		1.59		83.7		1.600		
		1.59		83.7		1.600		
	82	1.12	1.11	84.8	84.8	1.125	1.121	0.0058
		1.11		84.8		1.115		
		1.12		84.8		1.125		
S2+2% 10A	70	2.71	2.7	83.5	83.5	2.728	2.717	0.0371
		2.66		83.7		2.676		
		2.73		83.4		2.748		
	73	1.86	1.85	84.6	84.6	1.868	1.858	0.0465
		1.8		84.8		1.807		
		1.89		84.5		1.899		
	76	1.3	1.29	85.5	85.5	1.304	1.297	0.0407
		1.25		85.6		1.254		
		1.33		85.4		1.334		
	79	0.921	0.92	86.3	86.2	0.923	0.927	0.0279
		0.9		86.3		0.902		
		0.955		86.2		0.957		
S2+3% 10A	70	2.88	2.87	83.5	83.5	2.899	2.895	0.0256
		2.9		83.5		2.919		
		2.85		83.6		2.868		
	73	1.99	1.98	84.5	84.5	1.999	1.996	0.0153
		2		84.5		2.009		
		1.97		84.5		1.979		
	76	1.4	1.39	85.4	85.4	1.405	1.398	0.0210
		1.41		85.4		1.415		
		1.37		85.5		1.374		
	79	0.997	0.99	86.2	86.2	0.999	0.998	0.0151
		1.01		86.2		1.012		
		0.98		86.2		0.982		
S2+1% 11B	73	2.47	2.47	82.9	82.9	2.489	2.492	0…..
		2.45		83		2.468		
		2.5		82.8		2.520		
	76	1.7	1.69	84	84.0	1.709	1.706	0.0256
		1.67		84.1		1.679		
		1.72		83.9		1.730		
	79	1.18	1.17	85	85.0	1.185	1.181	0.0254
		1.15		85.1		1.154		
		1.2		85		1.205		

Sample Name	Temp. (C)	G* (kPa)	Avg.	Phase Angle, δ	Avg.	G*/sinδ (kPa)	Avg.	St Deviation
	82	0.832	0.831	86	86.0	0.834	0.833	0.0196
		0.811		86		0.813		
		0.85		86		0.852		
S2+2% 11B	73	2.65	2.64	82.9	82.9	2.670	2.667	0.0157
		2.66		82.9		2.681		
S2+2% 11B	73	2.63	2.64	83	82.9	2.650	2.667	0.0157
	76	1.82	1.81	84.1	84.1	1.830	1.826	0.0155
		1.83		84.1		1.840		
		1.8		84.2		1.809		
	79	1.27	1.26	85.1	85.1	1.275	1.268	0.0116
		1.27		85.1		1.275		
		1.25		85.1		1.255		
	82	0.895	0.89	86	86	0.897	0.892	0.0087
		0.895		86		0.897		
		0.88		86		0.882		
S2+3% 11B	73	2.5	2.49	83.5	83.5	2.516	2.513	0.0058
		2.49		83.5		2.506		
		2.5		83.5		2.516		
	76	1.74	1.73	84.5	84.5	1.748	1.745	0.0153
		1.72		84.5		1.728		
		1.75		84.5		1.758		
	79	1.22	1.21	85.5	85.4	1.224	1.220	0.0154
		1.2		85.5		1.204		
		1.23		85.4		1.234		
	82	0.872	0.865	86.3	86.3	0.874	0.867	0.0131
		0.85		86.4		0.852		
		0.873		86.3		0.875		
S2+1% 15A	73	2.1	2.10	83.3	83.2	2.114	2.118	0.0061
		2.1		83.3		2.114		
		2.11		83.2		2.125		
	76	1.45	1.45	84.3	84.27	1.457	1.461	0.0060
		1.45		84.3		1.457		
		1.46		84.2		1.468		
	79	1.01	1.01	85.3	85.2	1.013	1.017	0.0059
		1.01		85.3		1.013		
		1.02		85.2		1.024		
	82	0.712	0.71	86.2	86.2	0.714	0.716	0.0046
		0.712		86.2		0.714		

Sample Name	Temp. (C)	G* (kPa)	Avg.	Phase Angle, δ	Avg.	G*/sinδ (kPa)	Avg.	St Deviation
		0.72		86.2		0.722		
S2+2% 15A	73	2.11	2.10	83.4	83.4	2.124	2.121	0.0156
		2.12		83.4		2.134		
		2.09		83.5		2.104		
	76	1.46	1.45	84.5	84.5	1.467	1.463	0.0155
S2+2% 15A	76	1.47	1.45	84.5	84.5	1.477	1.463	0.0155
		1.44		84.6		1.446		
	79	1.02	1.02	85.4	85.4	1.023	1.023	0.0100
		1.03		85.4		1.033		
		1.01		85.4		1.013		
	82	0.724	0.72	86.2	86.2	0.726	0.726	0.0065
		0.731		86.2		0.733		
		0.718		86.2		0.720		
S2+3% 15A	70	2.89	2.91	82.6	82.5	2.914	2.938	0.0261
		2.91		82.5		2.935		
		2.94		82.4		2.966		
	73	1.99	2.00	83.5	83.4	2.003	2.020	0.0212
		2		83.5		2.013		
		2.03		83.4		2.044		
	76	1.38	1.39	84.5	84.8	1.386	1.399	0.0143
		1.39		84.5		1.396		
		1.41		85.4		1.415		
	79	0.978	0.97	85.3	85.2	0.981	0.983	0.0022
		0.979		85.3		0.982		
		0.9*82*		85.2		0.985		

Table C.2. Table dynamic shear rheometer (DSR) test results RTFO: aged binders.

Temp. (C)	G* (kPa)	Avg.	Phase Angle, δ	Avg.	G*/sinδ (kPa)	Avg.	St Deviation
64	4.59	4.45	80.1	80.33	4.660	4.517	0.1240
	4.38		80.6		4.440		
	4.39		80.3		4.450		
67	3.13	3.04	81.4	81.6	3.160	3.070	0.0781
	3		81.8		3.030		
	2.99		81.6		3.020		
70	2.15	2.09	82.6	82.8	2.170	2.113	0.0493
	2.07		83		2.090		
	2.06		82.8		2.080		
S1+1%	10A						
76	4.04	4.24	77.8	77.367	4.133	4.346	0.2425
	4.19		77.4		4.293		
	4.49		76.9		4.610		
79	2.82	2.97	79.3	79.167	2.870	3.028	0.174
	2.95		79.8		2.997		
	3.15		78.4		3.216		
82	1.99	2.10	80.7	80.3	2.017	2.137	0.130
	2.09		80.3		2.120		
	2.24		79.9		2.275		
S1+2%	10A						
76	4.89	5.03	76.6	76.367	5.027	5.176	0.323
	4.82		76.6		4.955		
	5.38		75.9		5.547		
79	3.45	3.55	78.1	77.867	3.526	3.635	0.234
	3.4		78.1		3.475		
	3.81		77.4		3.904		
82	2.46	2.53	79.5	79.233	2.502	2.576	0.163
	2.42		79.4		2.462		
	2.71		78.8		2.763		
S1+3%	10A						
73	4.05	3.96	79.3	79.467	4.122	4.035	0.115
	3.84		79.6		3.904		
	4.01		79.5		4.078		
76	2.84	2.79	80.5	80.367	2.879	2.833	0.049
	2.74		80.1		2.781		
	2.8		80.5		2.839		
79	2.04	1.99	81.7	81.8	2.062	2.017	0.038

Temp. (C)	G* (kPa)	Avg.	Phase Angle, δ	Avg.	G*/sinδ (kPa)	Avg.	St Deviation
	1.97		81.9		1.990		
	1.98		81.8		2.000		
S1+1%	11B						
76	5.38	5.33	75.2	75.133	5.565	5.518	0.041
	5.3		75		5.487		
	5.32		75.2		5.503		
79	3.77	3.75	76.8	76.9	3.872	3.854	0.041
	3.78		76.8		3.883		
	3.71		77.1		3.806		
82	2.65	2.61	78.4	78.733	2.705	2.668	0.032
	2.6		78.9		2.650		
	2.6		78.9		2.650		
S1+2%	11B						
76	3.66	3.65	78.9	78.833	3.730	3.721	0.060
	3.7		78.5		3.776		
	3.59		79.1		3.656		
79	2.56	2.53	80.3	80.433	2.597	2.572	0.0348
	2.5		80.7		2.533		
	2.55		80.3		2.587		
82	1.89	1.82	81.6	81.833	1.910	1.842	0.0629
	1.81		81.7		1.829		
	1.77		82.2		1.787		
S1+3%	11B						
76	3.2	3.25	80.5	80.2	3.244	3.305	0.054
	3.27		80.1		3.319		
	3.3		80		3.351		
79	2.3	2.27	81.5	81.633	2.326	2.298	0.039
	2.29		81.5		2.315		
	2.23		81.9		2.252		
82	1.62	1.61	82.7	82.7	1.633	1.627	0.012
	1.62		82.7		1.633		
	1.6		82.7		1.613		
S1+1%	15A						
76	4.29	4.62	76.3	75.867	4.416	4.765	0.312
	4.71		75.8		4.858		
	4.86		75.5		5.020		
79	3	3.23	78	77.533	3.067	3.312	0.218
	3.3		77.5		3.380		

Temp. (C)	G* (kPa)	Avg.	Phase Angle, δ	Avg.	G*/sinδ (kPa)	Avg.	St Deviation
	3.4		77.1		3.488		
82	2.11	2.27	79.5	79.067	2.146	2.319	0.153
	2.33		79		2.374		
	2.39		78.7		2.437		
S1+2%	15A						
76	4.22	4.20	77.1	77.3	4.329	4.312	0.061
	4.15		77.9		4.244		
	4.25		76.9		4.364		
79	2.95	2.96	78.7	78.633	3.008	3.027	0.138
	3.1		77.7		3.173		
	2.85		79.5		2.899		
82	2.09	2.07	80.1	79.967	2.122	2.103	0.099
	1.97		81		1.995		
	2.15		78.8		2.192		
S1+3%	15A						
76	3.59	3.55	78.7	78.567	3.661	3.629	0.128
	3.43		79.5		3.488		
	3.65		77.5		3.739		
79	2.51	2.49	80.2	80.267	2.547	2.533	0.024
	2.51		80.1		2.548		
	2.47		80.5		2.504		
82	1.77	1.79	81.5	81.333	1.790	1.811	0.107
	1.9		80.2		1.928		
	1.7		82.3		1.715		
S2							
64	3.94	3.84	83.2	83.267	3.968	3.867	0.092
	3.76		83.3		3.786		
	3.82		83.3		3.846		
67	2.54	2.58333333	84.3	84.267	2.553	2.596	0.0599
	2.65		84.2		2.664		
	2.56		84.3		2.573		
70	1.75	1.77	85.2	85.2	1.756	1.776	0.034
	1.81		85.1		1.817		
	1.75		85.3		1.756		
S2+1%	10A						
76	3.72	3.92666667	79.8	79.367	3.780	3.995	0.189
	4		79.2		4.072		
	4.06		79.1		4.135		

Temp. (C)	G* (kPa)	Avg.	Phase Angle, δ	Avg.	G*/sinδ (kPa)	Avg.	St Deviation
79	2.58	2.71	81.3	80.867	2.610	2.745	0.1196
	2.75		80.7		2.787		
	2.8		80.6		2.838		
82	1.8	1.89	82.6	82.2	1.815	1.908	0.084
	1.91		82.1		1.928		
	1.96		81.9		1.980		
S2+2%	10A						
70	4.28	4.58	81.5	81.2	4.328	4.641	0.278
	4.8		81		4.860		
	4.68		81.1		4.737		
73	2.93	3.12	82.8	82.467	2.953	3.151	0.173
	3.25		82.3		3.280		
	3.19		82.3		3.219		
76	2.04	2.16	83.8	83.567	2.052	2.177	0.109
	2.24		83.4		2.255		
	2.21		83.5		2.224		
79		1.55		84.5		1.562	0.021
	1.57		84.5		1.577		
	1.54		84.5		1.547		
S2+3%	10A						
70	4.51	4.51	81.6	81.533	4.559	4.567	0.114
	4.63		81.2		4.685		
	4.41		81.8		4.456		
73	3.07	3.07	82.8	82.8	3.094	3.098	0.087
	3.16		82.6		3.187		
	2.99		83		3.012		
76	2.13	2.14	83.9	83.767	2.142	2.159	0.058
	2.21		83.5		2.224		
	2.1		83.9		2.112		
S2+1%	11B						
73	3.74	3.71	80.7	80.733	3.790	3.759	0.054
	3.65		80.9		3.697		
	3.74		80.6		3.791		
76	2.56	2.54	82	82.067	2.585	2.568	0.038
	2.5		82.2		2.523		
	2.57		82		2.595		
79	1.77	1.76	83.3	83.3	1.782	1.779	0.025
	1.74		83.4		1.752		

Temp. (C)	G* (kPa)	Avg.	Phase Angle, δ	Avg.	G*/sinδ (kPa)	Avg.	St Deviation
	1.79		83.2		1.803		
S2+2%	11B						
73	3.72	3.77	81.1	81.1	3.765	3.816	0.044
	3.8		81.1		3.846		
	3.79		81.1		3.836		
76	2.55	2.59	82.4	82.4	2.573	2.613	0.036
	2.62		82.4		2.643		
	2.6		82.4		2.623		
79	1.76	1.79	83.6	83.6	1.771	1.808	0.035
	1.83		83.6		1.841		
	1.8		83.6		1.811		
S2+3%	11B						
73	3.77	3.67	81.6	81.8	3.811	3.708	0.091
	3.6		81.9		3.636		
	3.64		81.9		3.677		
76	2.58	2.52	82.9	83.067	2.600	2.545	0.051
	2.48		83.2		2.498		
	2.52		83.1		2.538		
79	1.8	1.76	84.1	84.167	1.810	1.776	0.0354
	1.73		84.2		1.739		
	1.77		84.2		1.779		
S2+1%	15A						
73	3.42	3.38	81	81.033	3.463	3.429	0.036
	3.35		81.1		3.391		
	3.39		81		3.432		
76	2.34	2.32	82.3	82.367	2.361	2.341	0.0204
	2.3		82.4		2.320		
	2.32		82.4		2.341		
79	1.63	1.61	83.5	83.567	1.641	1.624	0.0154
	1.6		83.6		1.610		
	1.61		83.6		1.620		
S2+2%	15A						
70	4.56	4.69	80.5	80.333	4.623	4.758	0.133
	4.69		80.3		4.758		
	4.82		80.2		4.891		
73	3.1	3.18	81.9	81.733	3.131	3.220	0.087
	3.19		81.7		3.224		
	3.27		81.6		3.305		

Temp. (C)	G* (kPa)	Avg.	Phase Angle, δ	Avg.	G*/sinδ (kPa)	Avg.	St Deviation
76	2.13	2.19	83.1	82.967	2.146	2.207	0.061
	2.19		83		2.206		
	2.25		82.8		2.268		
79		1.55		84.05		1.558	0.028
	1.53		84.1		1.538		
	1.57		84		1.579		
S2+3%	15A						
70	4.46	4.53	80.8	80.7	4.518	4.590	0.098
	4.49		80.7		4.550		
	4.64		80.6		4.703		
73	3.03	3.08	82.2	82.067	3.058	3.113	0.069
	3.06		82.1		3.089		
	3.16		81.9		3.192		
76	2.08	2.12	83.4	83.267	2.094	2.135	0.046
	2.11		83.3		2.125		
	2.17		83.1		2.186		

APPENDIX D. A AND VTS CALCULATION FROM DSR RESULTS

Table D.1. Table A and VTS calculation from DSR results.

Temp.	Phase Angle	Complex Shear Modulus	Visc.	Temperature T (Rankine)	Log T (R)	Log (Log(η))
S1+1% 10A			A = 21.68	VTS = -7.62		
61	74.2	14.6	1760.72	601.47	2.78	0.51
64	75.7	9.9	1153.73	606.87	2.78	0.49
67	77.2	6.69	756.09	612.27	2.79	0.46
70	78.8	4.5	494.11	617.67	2.79	0.43
73	80.2	3.09	331.90	623.07	2.79	0.40
76	81.5	2.15	226.86	628.47	2.80	0.37
79	82.6	1.51	157.27	633.87	2.80	0.34
82	83.7	1.07	110.20	639.27	2.81	0.31
S1+2% 10A			A = 20.56	VTS = -7.21		
61	72.8	18.2	2273.50	601.47	2.78	0.53
64	74.5	12.1	1448.86	606.87	2.78	0.50
67	76	8.19	948.34	612.27	2.79	0.47
70	77.5	5.69	639.40	617.67	2.79	0.45
73	79	3.94	431.18	623.07	2.79	0.42
76	80.4	2.75	294.52	628.47	2.80	0.39
79	81.6	1.95	205.50	633.87	2.80	0.36
82	82.8	1.39	144.46	639.27	2.81	0.33
S1+3% 10A			A = 20.82	VTS = -7.32		
61	77.5	9.71	1091.14	601.47	2.78	0.48
64	78.8	6.62	726.89	606.87	2.78	0.46
67	80	4.52	486.93	612.27	2.79	0.43
70	81.2	3.14	332.61	617.67	2.79	0.40
73	82.3	2.21	230.95	623.07	2.79	0.37
76	83.2	1.64	169.73	628.47	2.80	0.35
79	84.2	1.17	119.96	633.87	2.80	0.32
82	85	0.86	87.61	639.27	2.81	0.29
S1+1% 11B			A = 20.94	VTS = -7.34		
61	71.5	18.6	2407.51	601.47	2.78	0.53
64	73.1	12.6	1561.72	606.87	2.78	0.50
67	74.7	8.54	1017.81	612.27	2.79	0.48
70	76.2	5.94	684.93	617.67	2.79	0.45
73	77.8	4.06	453.70	623.07	2.79	0.42
76	79.3	2.8	304.93	628.47	2.80	0.40
79	80.6	1.95	208.25	633.87	2.80	0.37

Temp.	Phase Angle	Complex Shear Modulus	Visc.	Temperature T (Rankine)	Log T (R)	Log (Log(η))
82	81.8	1.38	145.07	639.27	2.81	0.33
S1+2% 11B			A = 21.65	VTS = -7.60		
61	74	15.2	1841.96	601.47	2.78	0.51
64	75.6	10.2	1191.28	606.87	2.78	0.49
67	77.1	6.89	780.20	612.27	2.79	0.46
70	78.7	4.66	512.54	617.67	2.79	0.43
73	80.2	3.2	343.71	623.07	2.79	0.40
76	81.5	2.22	234.25	628.47	2.80	0.37
79	82.7	1.56	162.30	633.87	2.80	0.34
82	83.9	1.1	113.08	639.27	2.81	0.31
S1+3% 11B			A = 21.50	VTS = -7.55		
61	75.4	13.7	1607.09	601.47	2.78	0.51
64	76.9	9.23	1049.27	606.87	2.78	0.48
67	78.4	6.21	686.55	612.27	2.79	0.45
70	79.9	4.22	455.30	617.67	2.79	0.42
73	81.2	2.93	310.37	623.07	2.79	0.40
76	82.4	2.04	212.94	628.47	2.80	0.37
79	83.5	1.45	149.62	633.87	2.80	0.34
82	84.5	1.03	105.34	639.27	2.81	0.31
S1+1% 15A			A = 21.55	VTS = -7.57		
61	72.1	15.9	2023.86	601.47	2.78	0.52
64	73.6	10.8	1321.74	606.87	2.78	0.49
67	75.2	7.42	874.29	612.27	2.79	0.47
70	76.9	4.95	562.72	617.67	2.79	0.44
73	78.4	3.42	378.10	623.07	2.79	0.41
76	79.8	2.36	255.01	628.47	2.80	0.38
79	81.1	1.65	175.01	633.87	2.80	0.35
82	82.1	1.17	122.55	639.27	2.81	0.32
S1+2% 15A			A = 21.51	VTS = -7.55		
61	72	16	2042.20	601.47	2.78	0.52
64	73.5	10.8	1325.05	606.87	2.78	0.49
67	75.1	7.41	875.08	612.27	2.79	0.47
70	76.7	4.99	569.53	617.67	2.79	0.44
73	78.2	3.42	379.43	623.07	2.79	0.41
76	79.5	2.37	257.28	628.47	2.80	0.38
79	80.7	1.66	177.03	633.87	2.80	0.35
82	81.7	1.17	123.15	639.27	2.81	0.32
S1+3% 15A			A = 21.63	VTS = -7.60		
61	73.8	13.8	1680.52	601.47	2.78	0.51

Temp.	Phase Angle	Complex Shear Modulus	Visc.	Temperature T (Rankine)	Log T (R)	Log (Log(η))
64	75.3	9.37	1101.60	606.87	2.78	0.48
67	76.9	6.39	726.42	612.27	2.79	0.46
70	78.4	4.31	476.50	617.67	2.79	0.43
73	79.8	2.97	320.92	623.07	2.79	0.40
76	81.1	2.07	219.56	628.47	2.80	0.37
79	82.2	1.46	152.75	633.87	2.80	0.34
82	83.2	1.04	107.63	639.27	2.81	0.31
S1			A = 23.76	VTS = -8.41		
61	84.8	2.44	248.94	601.47	2.78	0.38
64	85.6	1.68	170.43	606.87	2.78	0.35
67	86.3	1.16	117.18	612.27	2.79	0.32
70	87	0.82	82.55	617.67	2.79	0.28
S2			A = 23.76	VTS = -8.41		
61	84.8	2.44	248.94	601.47	2.78	0.38
64	85.6	1.66	168.40	606.87	2.78	0.35
67	86.3	1.14	115.16	612.27	2.79	0.31
S2+1% 10A			A = 22.09	VTS = -7.76		
61	75	16.8	1988.49	601.47	2.78	0.52
64	76.6	11.2	1280.88	606.87	2.78	0.49
67	78.2	7.44	825.43	612.27	2.79	0.46
70	79.8	4.95	534.87	617.67	2.79	0.44
73	81.2	3.35	354.86	623.07	2.79	0.41
76	82.5	2.29	238.77	628.47	2.80	0.38
79	83.7	1.59	163.75	633.87	2.80	0.35
82	84.8	1.12	114.27	639.27	2.81	0.31
S2+2% 10A			A = 22.69	VTS = -7.99		
61	79.9	9.09	980.73	601.47	2.78	0.48
64	81.1	6.03	639.59	606.87	2.78	0.45
67	82.4	4.05	422.75	612.27	2.79	0.42
70	83.5	2.71	279.63	617.67	2.79	0.39
73	84.6	1.86	190.07	623.07	2.79	0.36
76	85.5	1.3	131.97	628.47	2.80	0.33
79	86.3	0.921	93.04	633.87	2.80	0.29
S2+3% 10A			A = 22.21	VTS = -7.82		
61	79.8	9.64	1041.65	601.47	2.78	0.48
64	81.1	6.37	675.65	606.87	2.78	0.45
67	82.3	4.29	448.32	612.27	2.79	0.42
70	83.5	2.88	297.17	617.67	2.79	0.39
73	84.5	1.99	203.52	623.07	2.79	0.36

Temp.	Phase Angle	Complex Shear Modulus	Visc.	Temperature T (Rankine)	Log T (R)	Log (Log(η))
76	85.4	1.4	142.21	628.47	2.80	0.33
79	86.2	0.997	100.77	633.87	2.80	0.30
S2+1% 11B			A = 20.94	VTS = -7.34		
61	77.2	12.4	1401.41	601.47	2.78	0.50
64	78.7	8.28	910.69	606.87	2.78	0.47
67	80.2	5.46	586.46	612.27	2.79	0.44
70	81.6	3.64	383.60	617.67	2.79	0.41
73	82.9	2.47	256.42	623.07	2.79	0.38
76	84	1.7	174.60	628.47	2.80	0.35
79	85	1.18	120.21	633.87	2.80	0.32
82	86	0.832	84.19	639.27	2.81	0.28
S2+2% 11B			A = 21.65	VTS = -7.60		
61	77.6	13.4	1502.98	601.47	2.78	0.50
64	78.8	8.89	976.14	606.87	2.78	0.48
67	80.2	5.89	632.64	612.27	2.79	0.45
70	81.7	3.9	410.49	617.67	2.79	0.42
73	82.9	2.65	275.11	623.07	2.79	0.39
76	84.1	1.82	186.76	628.47	2.80	0.36
79	85.1	1.27	129.28	633.87	2.80	0.32
82	86	0.895	90.57	639.27	2.81	0.29
S2+3% 11B			A = 21.50	VTS = -7.55		
61	78.2	12.5	1386.81	601.47	2.78	0.50
64	79.6	8.26	895.29	606.87	2.78	0.47
67	81	5.48	582.03	612.27	2.79	0.44
70	82.3	3.65	381.44	617.67	2.79	0.41
73	83.5	2.5	257.96	623.07	2.79	0.38
76	84.5	1.74	177.95	628.47	2.80	0.35
79	85.5	1.22	123.85	633.87	2.80	0.32
82	86.3	0.872	88.09	639.27	2.81	0.29
S2+1% 15A			A = 21.55	VTS = -7.57		
61	77.8	10.4	1162.18	601.47	2.78	0.49
64	79.3	6.91	752.52	606.87	2.78	0.46
67	80.7	4.63	493.77	612.27	2.79	0.43
70	82.1	3.07	321.57	617.67	2.79	0.40
73	83.3	2.1	217.12	623.07	2.79	0.37
76	84.3	1.45	148.54	628.47	2.80	0.34
79	85.3	1.01	102.67	633.87	2.80	0.30
82	86.2	0.712	71.97	639.27	2.81	0.27
S2+2% 15A			A = 21.51	VTS = -7.55		

Temp.	Phase Angle	Complex Shear Modulus	Visc.	Temperature T (Rankine)	Log T (R)	Log (Log(η))
61	78.1	10.3	1144.77	601.47	2.78	0.49
64	79.5	6.92	751.22	606.87	2.78	0.46
67	80.9	4.6	489.22	612.27	2.79	0.43
70	82.3	3.09	322.91	617.67	2.79	0.40
73	83.4	2.11	217.93	623.07	2.79	0.37
76	84.5	1.46	149.31	628.47	2.80	0.34
79	85.4	1.02	103.61	633.87	2.80	0.30
82	86.2	0.724	73.18	639.27	2.81	0.27
S2+3% 15A			A = 21.63	VTS = -7.60		
61	78.5	9.66	1066.12	601.47	2.78	0.48
64	79.9	6.42	692.66	606.87	2.78	0.45
67	81.2	4.35	460.78	612.27	2.79	0.43
70	82.5	2.91	303.42	617.67	2.79	0.39
73	83.5	2	206.37	623.07	2.79	0.36
76	84.5	1.39	142.15	628.47	2.80	0.33
79	85.3	0.979	99.52	633.87	2.80	0.30

APPENDIX E. SESSILE DROP EXPERIMENT

Table E.1. Contact angles for asphalt binders from Source 1.

Binder Type	Avg. Angle w/ Glycerin	Std. Deviation w/ Glycerin	Avg. Angle w/ Water	Std. Deviation w/ Water	Avg. Angle w/ Formamide	Std. Deviation w/ Formamide
PG 64-22	100.72	0.15	80.45	0.17	75.79	0.26
PG 64-22+1%Cloissite®10A	102.51	0.16	81.97	0.19	85.58	0.25
PG 64-22+2%Cloisite® 10A	103.42	0.23	80.47	0.15	81.25	0.23
PG 64-22+3%Cloisite® 10A	100.10	0.17	80.47	0.18	79.90	0.27
PG 64-22+1%Cloisite® 11B	102.28	0.17	81.68	0.21	84.54	0.25
PG 64-22+2%Cloisite® 11B	101.48	0.15	81.28	0.15	79.77	0.24
PG 64-22+3%Cloisite® 11B	100.94	0.36	81.96	0.15	80.07	0.24
PG 64-22+1%Cloisite® 15A	99.77	0.82	80.44	0.38	82.38	0.23
PG 64-22+2%Cloisite® 15A	98.93	0.20	81.68	0.18	80.84	0.23
PG 64-22+3%Cloisite® 15A	101.47	0.19	80.74	0.17	80.68	0.23

Table E.2. Contact angles for asphalt binders from Source 2.

Binder Type	Avg. Angle w/ Glycerin	Std. Deviation w/ Glycerin	Avg. Angle w/ Water	Std. Deviation w/ Water	Avg. Angle w/ Formamide	Std. Deviation w/ Formamide
PG 64-22	97.32	0.88	81.95	0.87	80.53	0.48
PG 64-22+1%Cloisite®10A	97.88	0.20	76.96	0.38	78.55	0.23
PG 64-22+2%Cloisite® 10A	97.50	0.23	77.41	0.44	79.87	0.22
PG 64-22+3%Cloisite® 10A	97.72	0.23	77.77	0.18	75.80	0.24
PG 64-22+1%Cloisite® 11B	97.90	0.24	75.60	0.36	77.96	0.23
PG 64-22+2%Cloisite® 11B	97.96	0.21	77.51	0.38	78.29	0.24
PG 64-22+3%Cloisite® 11B	99.45	0.21	77.89	0.15	80.59	0.20
PG 64-22+1%Cloisite® 15A	97.14	0.35	76.60	0.48	77.77	0.22
PG 64-22+2%Cloisite® 15A	98.68	0.21	76.85	0.19	79.26	0.22
PG 64-22+3%Cloisite® 15A	98.49	0.21	78.86	0.32	78.94	0.21

Table E.3. Contact angles for asphalt binders from Source 2.

Binder Type	Aging	Γ^{lw}	Γ_L^-	Γ^+	Γ^{ab}	Γ	$\Gamma^+/\Gamma L-$
PG 64-22	Un-aged	7.27	2.17	3.62	5.61	12.88	1.67
PG 64-22+1% Cloisite® 10A	Un-aged	10.00	1.83	1.88	3.71	13.71	1.03
PG 64-22+2% Cloisite® 10A	Un-aged	10.11	1.69	1.68	3.37	13.48	0.99
PG 64-22+3% Cloisite® 10A	Un-aged	10.25	2.24	2.21	4.45	14.70	0.99
PG 64-22+1% Cloisite® 11B	Un-aged	10.09	1.93	1.82	3.75	13.84	0.94
PG 64-22+2% Cloisite® 11B	Un-aged	9.86	2.41	1.74	4.10	13.96	0.72
PG 64-22+3% Cloisite® 11B	Un-aged	7.31	2.11	3.57	5.49	12.80	1.69
PG 64-22+1% Cloisite® 15A	Un-aged	7.42	2.34	3.75	5.92	13.34	1.60
PG 64-22+2% Cloisite® 15A	Un-aged	7.51	2.51	3.88	6.24	13.75	1.55
PG 64-22+3% Cloisite® 15A	Un-aged	7.20	2.02	3.51	5.33	12.53	1.74

Table E.4. Cohesive energy for Source 1 binders.

Asphalt Sample	Cohesive Energy
PG 64-22	25.75
PG 64-22+1% Cloisite® 10A	27.42
PG 64-22+2% Cloisite® 10A	26.96
PG 64-22+3% Cloisite® 10A	29.40
PG 64-22+1% Cloisite® 11B	27.68
PG 64-22+2% Cloisite® 11B	27.91
PG 64-22+3% Cloisite® 11B	25.60
PG 64-22+1% Cloisite® 15A	26.69
PG 64-22+2% Cloisite® 15A	27.50
PG 64-22+3%Cloisite ® 15A	25.75

Table E.5. Cohesive energy for modified asphalt binder sample of Source 1.

Binder Type	Aging	Γ^{lw}	Γ_L^-	Γ^+	Γab	Γ	$\Gamma^+/\Gamma L-$
PG 64-22	Un-aged	10.27	2.75	2.78	5.53	15.80	1.01
PG 64-22+1% Cloisite® 10A	Un-aged	10.24	2.64	2.68	5.32	15.56	1.02
PG 64-22+2% Cloisite® 10A	Un-aged	10.27	2.71	2.75	5.46	15.73	1.01
PG 64-22+3% Cloisite® 10A	Un-aged	10.25	2.67	2.71	5.38	15.63	1.01
PG 64-22+1% Cloisite® 11B	Un-aged	10.23	2.64	2.67	5.31	15.54	1.01
PG 64-22+2% Cloisite® 11B	Un-aged	10.23	2.63	2.66	5.29	15.52	1.01
PG 64-22+3% Cloisite® 11B	Un-aged	10.11	2.36	2.40	4.76	14.87	1.02
PG 64-22+1% Cloisite® 15A	Un-aged	10.29	2.78	2.82	5.60	15.89	1.01
PG 64-22+2% Cloisite® 15A	Un-aged	10.15	2.50	2.54	5.04	15.19	1.02
PG 64-22+3% Cloisite® 15A	Un-aged	10.17	2.54	2.57	5.11	15.28	1.01

Table E.6. Cohesive energy for modified asphalt binder sample of Source 2.

Asphalt Sample	Cohesive Energy
PG 64-22	31.60
PG 64-22+1% Cloisite® 10A	31.12
PG 64-22+2% Cloisite® 10A	31.46
PG 64-22+3% Cloisite® 10A	31.26
PG 64-22+1% Cloisite® 11B	31.08
PG 64-22+2% Cloisite® 11B	31.04
PG 64-22+3% Cloisite® 11B	29.74
PG 64-22+1% Cloisite® 15A	31.78
PG 64-22+2% Cloisite® 15A	30.38
PG 64-22++3% Cloisite® 15A	30.56

Table E.7. Source 1 binder properties with sandstone.

Sample	Delta G (Dry)	Dry	Wet	Dry/Wet	Dry/Wet
PG 64-22	125.22868	125.2	-131.2	0.9542683	0.95
PG 64-22+1% Cloisite® 10A	120.69582	120.7	-148.3	0.8138908	0.81
PG 64-22+2% Cloisite® 10A	116.83051	116.8	-154.0	0.7584416	0.76
PG 64-22+3% Cloisite® 10A	128.18406	128.2	-154.0	0.8324675	0.83
PG 64-22+1% Cloisite® 11B	120.23099	120.2	-154.0	0.7805195	0.78
PG 64-22+2% Cloisite® 11B	120.07072	120.1	-154.0	0.7798701	0.78
PG 64-22+3% Cloisite® 11B	140.13253	140.1	-181.0	0.7740331	0.77
PG 64-22+1% Cloisite® 15A	143.43608	143.4	-226.6	0.6328332	0.63
PG 64-22+2% Cloisite® 15A	145.80147	145.8	-175.9	0.82888	0.83
PG 64-22+3% Cloisite® 15A	138.77916	138.8	-201.8	0.6878097	0.69

Table E.8. Source 2 binder properties with sandstone.

Sample	Delta G (Dry)	Dry	Wet	Dry/Wet	Dry/Wet
PG 64-22	140.87400	140.9	-57.4	2.4547038	2.45
PG 64-22+1% Cloisite® 10A	120.69582	120.7	-59.3	2.0354132	2.04
PG 64-22+2% Cloisite® 10A	141.55189	141.6	-55.3	2.5605787	2.56
PG 64-22+3% Cloisite® 10A	155.65288	155.7	-52.6	2.960076	2.96
PG 64-22+1% Cloisite® 11B	145.66198	145.7	-27.1	5.3763838	5.38
PG 64-22+2% Cloisite® 11B	144.80434	144.8	-37.3	3.8820375	3.88
PG 64-22+3% Cloisite® 11B	172.81103	172.8	-29.9	5.7792642	5.78
PG 64-22+1% Cloisite® 15A	176.79321	176.8	-33.7	5.2462908	5.25
PG 64-22+2% Cloisite® 15A	179.64281	179.6	-34.4	5.2209302	5.22
PG 64-22+3% Cloisite® 15A	171.20623	171.2	-33.5	5.1104478	5.11

Table E.9. Source 1 binder properties with gravel.

Sample	Delta G (Dry)	Dry	Wet	Dry/Wet	Dry/Wet
PG 64-22	168.52549	168.5	-118.0	1.4279661	1.43
PG 64-22+1% Cloisite® 10A	166.24512	166.2	-148.7	1.1176866	1.12
PG 64-22+2% Cloisite® 10A	137.90520	137.9	-115.7	1.1918755	1.19
PG 64-22+3% Cloisite® 10A	137.16407	137.2	-132.6	1.0346908	1.03
PG 64-22+1% Cloisite® 11B	136.45041	136.5	-134.5	1.0148699	1.01
PG 64-22+2% Cloisite® 11B	136.27336	136.3	-125.4	1.0869219	1.09
PG 64-22+3% Cloisite® 11B	131.26429	131.3	-61.1	2.1489362	2.15
PG 64-22+1% Cloisite® 15A	139.15908	139.2	-76.6	1.8172324	1.82
PG 64-22+2% Cloisite® 15A	133.92332	133.9	-61.3	2.1843393	2.18
PG 64-22+3% Cloisite® 15A	134.54075	134.5	-69.2	1.9436416	1.94

Table E.10 Source 2 binder properties with gravel.

Sample	Delta G (Dry)	Dry	Wet	Dry/Wet	Dry/Wet
PG 64-22	138.45887	138.5	-70.4	1.9673295	1.97
PG 64-22+1% Cloisite® 10A	136.61510	136.6	-67.3	2.0297177	2.03
PG 64-22+2% Cloisite® 10A	167.84661	167.8	-40.5	4.1432099	4.14
PG 64-22+3% Cloisite® 10A	166.92715	166.9	-51.7	3.2282398	3.23
PG 64-22+1% Cloisite® 11B	166.03070	166.0	-41.9	3.9618138	3.96
PG 64-22+2% Cloisite® 11B	165.81008	165.8	-47.0	3.5276596	3.53
PG 64-22+3% Cloisite® 11B	159.60417	159.6	-47.8	3.3389121	3.34
PG 64-22+1% Cloisite® 15A	169.40497	169.4	-46.4	3.6508621	3.65
PG 64-22+2% Cloisite® 15A	162.90917	162.9	-52.4	3.1087786	3.11
PG 64-22+3% Cloisite® 15A	163.66304	163.7	-69.6	2.3520115	2.35

Table E.11. Compatibility ratio for Source 1 binders.

Binder Type	Sandstone	Gravel
PG 64-22	0.95	2.45
PG 64-22+1% Cloisite® 10A	0.81	2.04
PG 64-22+2% Cloisite® 10A	0.76	2.56
PG 64-22+3% Cloisite® 10A	0.83	2.96
PG 64-22+1% Cloisite® 11B	0.78	5.38
PG 64-22+2% Cloisite® 11B	0.78	3.88
PG 64-22+3% Cloisite® 11B	0.77	5.78
PG 64-22+1% Cloisite® 15A	0.63	5.25
PG 64-22+2% Cloisite® 15A	0.83	5.22
PG 64-22+3% Cloisite® 15A	0.69	5.11

Table E.12. Compatibility ratio for Source 2 binders.

Binder Type	Sandstone	Gravel
PG 64-22	1.43	1.97
PG 64-22+1% Cloisite® 10A	1.12	2.03
PG 64-22+2% Cloisite® 10A	1.19	4.14
PG 64-22+3% Cloisite® 10A	1.03	3.23
PG 64-22+1% Cloisite® 11B	1.01	3.96
PG 64-22+2% Cloisite® 11B	1.09	3.53
PG 64-22+3% Cloisite® 11B	2.15	3.34
PG 64-22+1% Cloisite® 15A	1.82	3.65
PG 64-22+2% Cloisite® 15A	2.18	3.11
PG 64-22+3% Cloisite® 15A	1.94	2.35

APPENDIX F. SARA ANALYSIS TEST RESULTS

Table F.1. SARA analysis for unaged binders.

Sample	Saturates (%)	Aromatics	Resin	Asphaltenes	% Recovered	Date
S1	10	38.3	31.8	19.9		
S1+1% 10A	11.9	26.5	31.1	30.5	96.5	5/28/2018
S1+2% 10A	8.1	37.3	34.3	20.3	93	5/28/2018
S1+3% 10A	6.1	28.7	30.8	34.4	90.8	1/2/2018
S1+1% 11B	10.7	37.4	33.5	18.4	98	5/23/2018
S1+2% 11B	8.1	35.1	26.2	30.6	99	1/8/2018
S1+3% 11B	5.6	30.3	33.9	30.2	94.7	5/23/2018
S1+1% 15A	5.7	33.9	30	30.4	98.7	1/3/2018
S1+2% 15A	9.4	27.2	38.6	24.8	96.2	5/25/2018
S1+3% 15A	9.8	33.1	29.5	27.6	94.8	1/5/2018
S2	6.8	43.6	36.3	13.2		
S2+1%10A	7.4	38.3	34.7	19.6	99.1	5/10/2018
S2+2%10A	5.6	28.3	30.9	35.2	94.7	5/13/2015
S2+3%10A	11.5	24.7	35.1	28.7	97.9	5/14/2018
S2+1% 11B	7.7	36.8	32.6	22.9	98.9	5/15/2018
S2+2% 11B	5	36.5	33.1	25.4	95.1	5/16/2018
S2+3% 11B	4.6	31.9	36.9	26.6	92.4	5/17/2018
S2+1% 15A	15.2	29.3	25.3	30.2	99	5/22/2018
S2+2% 15A	2.6	31.2	35.9	30.3	98.3	5/23/2018
S2+3%15A	10.2	25.6	29.1	35.1	93.02	5/21/2018